

DESIGN AND FATIGUE ANALYSIS OF AN LWD DRILL TOOL

A Thesis

Submitted to the Faculty

of

Purdue University

by

Riddhi Joshi

In Partial Fulfillment of the

Requirements for the Degree

of

Master of Science in Mechanical Engineering

August 2019

Purdue University

Indianapolis, Indiana

THE PURDUE UNIVERSITY GRADUATE SCHOOL
STATEMENT OF COMMITTEE APPROVAL

Dr. Hazim El-Mounayri, Chair

Department of Mechanical and Energy Engineering

Dr. Andres Tovar

Department of Mechanical and Energy Engineering

Dr. Khosrow Nematollahi

Department of Mechanical and Energy Engineering

Approved by:

Dr. Jie Chen

Head of the Graduate Program

To Mom and Dad.

ACKNOWLEDGMENTS

Foremost, I would like to thank Halliburton and Mr. Shashi Talya ,for offering me the Co-op opportunities in his group, under the Sperry drilling division and leading me working on diverse exciting projects.

I would like to express my sincere gratitude to my advisor Dr. Hazim El-Mounayri for the continuous support of my thesis study and research, for his patience, motivation, enthusiasm, and immense knowledge. His guidance helped me in all the time of research and writing of this thesis. I could not have imagined having a better advisor and mentor for my thesis study. Besides my advisor, I would like to thank the rest of my thesis committee: Prof. Andres Tovar and Prof. Khosrow Nematollahi, for their encouragement, insightful comments, and engaging questions.

I thank my fellow classmates: Somesh Rath, Meghana Kamble, John Thakidiyel and Viraj Gandhi for the stimulating discussions and the appreciable help they offered me to finish my thesis before the deadline.

Last but not the least, I would like to thank my family: my parents Neeta Joshi and Mukesh Joshi, for supporting me throughout my thesis and motivating me at times of adversity.

TABLE OF CONTENTS

	Page
LIST OF TABLES	vii
LIST OF FIGURES	viii
SYMBOLS	xi
ABBREVIATIONS	xii
ABSTRACT	xiii
1 INTRODUCTION	1
1.1 LWD Downhole Tool	1
1.2 Properties LWD Technology	3
1.3 Acoustic Imaging	4
1.4 Transducer	5
1.5 Project Scope and Layout	6
1.6 Problem Statement	7
1.7 Organisation of Report	8
2 LITERATURE REVIEW	9
2.1 Studies on Turbine Blade	9
2.2 Failure Analysis of a Drill Pipe	10
2.3 Fluctuating Stress Studies of a Dove-Tail Joint	12
2.4 Optimization and Fatigue Analysis of Differential	13
2.5 Previous Analysis of Baseline Tool	13
2.6 Summary of Previous Works	14
3 METHODOLOGY	15
3.1 The CAD Model	15
3.2 Types of Load Applied	17
3.3 Material Properties	19

	Page
3.4 Design of an LWD Drill Tool	20
3.5 Fatigue Life	22
3.5.1 Stress-Life Method	24
3.5.2 Endurance Limit Calculation	24
3.5.3 Fatigue Failure Theories	36
4 FEA MODEL SETUP	41
4.1 FEA Model Set-up for Fatigue Analysis of the Drill Tool	41
4.2 Meshing of Elements	41
4.3 Boundary Conditions	45
4.4 Parameterization	48
5 USER-DEFINED RESULTS AND CONCLUSION	53
5.1 Global Model (Von – Mises Stress)	53
5.1.1 Equivalent Stress	53
5.1.2 Total Deformation	53
5.2 Torque Only Load	54
5.2.1 Equivalent Stress	54
5.2.2 Total Deformation	55
5.3 Bending Moment Only	56
5.3.1 Equivalent Stress	56
5.3.2 Total Deformation	56
5.4 User Defined Results	57
5.4.1 Goodman Theory	57
5.4.2 Gerber Theory	58
5.5 Pressure Only	59
5.5.1 Equivalent Stress	59
5.5.2 Total Deformation	59
5.6 Limitations	60
REFERENCES	61

LIST OF TABLES

Table	Page
3.1 Composition of metals in Inconel 718	20
3.2 Mechanical properties of Inconel at different temperatures	21
3.3 Surface Correction Co-efficient 'a' and 'b'	26
3.4 Reliability Factor as given in Shigley book of Machine Design	28
3.5 Endurance Limit factor	30
3.6 Reliability correction factor (FKM guideline)	31
3.7 Size Correction Factor (FKM guideline)	32
3.8 List of a_R and $S_{t,u,min}$ (adopted from FKM Guideline)	34
3.9 Comparison of Guidelines for Endurance Limit	34
4.1 Load steps for Alternating Stress applying through Bending Moment	46
4.2 Data for different design point of the drill tool	49

LIST OF FIGURES

Figure	Page
1.1 Basic setup of BHA	2
1.2 Transducer application in the LWD tool and a Wire line tool	4
1.3 Two ultrasonic images are obtained by mapping the measured travel time and attenuation	5
1.4 Comparison of signal amplitude vs. borehole diameter	6
2.1 CAD model and FEA model of a turbine blade	10
2.2 Critical fatigue regions of the drill stem and connection	11
2.3 AFR model for the at-bit measurement	12
2.4 Dovetail Joint	13
2.5 Equivalent stress for rotating bending moment applied on the baseline tool	14
3.1 Workflow of the project	15
3.2 Isometric View of imaging pocket	16
3.3 Top View of imaging pocket	16
3.4 Cross-sectional view along the XZ plane	16
3.5 Loads acting on the drill tool	17
3.6 Tension and Compression on the tool	18
3.7 Flex for deflection of the drill tool	18
3.8 Rotational Torque acting on the tool	19
3.9 Data from Fatigue Design Handbook, SAE, 1968	25
3.10 Effective diameter for different cases	33
3.11 Surface correction factors	35
3.12 Trend of roughness correction factor against Material tensile strength using Shigley 2014 and FKM guideline	36
3.13 Trend of size correction factor against diameter using Shigley 1983, Shigley 2014 and FKM guideline	36

Figure	Page
3.14 Trend of temperature correction factor against temperature using Shigley 1983, Shigley 2014 and FKM guideline	36
3.15 Combined alternating and mean stress	37
3.16 Comparison of Soderberg, Goodman, and Gerber models	38
3.17 Failure point depiction in the design of cyclic load	40
4.1 Meshing of the LWD drill tool	42
4.2 Face sizing of one imaging pocket in tension	42
4.3 Face sizing 2 of one imaging pocket in tension	43
4.4 Assignment of pocket through named selection	44
4.5 Assignment of remote point through face selection	44
4.6 Environmental Condition in Workbench Simulation	45
4.7 Boundary condition for pressure only simulation	45
4.8 Boundary condition for rotating bending simulation	46
4.9 Boundary condition for torque only simulation	47
4.10 Images/Side view and Front view of boundary condition acting of the LWD tool for all three loads	48
4.11 Alternating stress vs Width of Imaging Pocket	50
4.12 Total Deformation vs Width of Imaging Pocket	51
4.13 Stress Life Theory vs Width of Imaging Pocket	52
4.14 Factor of Safety vs Width of Imaging Pocket	52
5.1 Equivalent Stress due to Global loading condition	54
5.2 Total deformation due to global loading	54
5.3 Equivalent load due to torque only load (mean stress)	55
5.4 Total deformation due to torque load	55
5.5 Equivalent stress due to alternating load by bending moment	56
5.6 Total deformation due to alternating load by bending moment	57
5.7 Simulation result for the user-defined result of Goodman Theory	57
5.8 Simulation result for the user-defined result of Goodman Theory	58
5.9 Graphical Solution	58

Figure	Page
5.10 Simulation result for the user-defined result of Goodman Theory	59
5.11 Simulation result for the user-defined result of Goodman Theory	60

SYMBOLS

S_{yt} tensile yield strength

S_{ut} ultimate tensile strength

k_a surface condition modification factor

k_b size modification factor

k_c load modification factor

k_d temperature modification factor

k_e reliability factor

k_f miscellaneous-effects modification factor

S_e endurance limit at the critical location of the geometry

S_e the endurance limit obtained from the rotating beam test

C_E endurance limit factor for materials

C_T temperature correction factor

C_R reliability factor

C_q roughness correction factor

$d_{eff,min}$ minimum effective diameter of component for the size correction factor

d_{eff} effective diameter of the component

R_z roughness coefficient

a_R roughness constant

σ_a stress amplitude/alternating stress

σ_m mean stress

σ_{max} maximum stress

σ_{min} minimum stress

ABBREVIATIONS

LWD	logging while drilling
MWD	measurement while drilling
BHA	bottom hole assembly
AFR	azimuthal focused resistivity
ABR	at-bit resistivity
ROP	rate of penetration
FKM	forschungskuratorium maschinenbau
W.O.B	weight on bit
RPM	revolution per minute
DLS	dog leg severity
FEA	finite element analysis
CAD	computer-aided design
DOE	design of experimentation
FEM	finite element manufacturing

ABSTRACT

Joshi, Riddhi. M.S.M.E., Purdue University, August 2019. Design and Fatigue Analysis of an LWD Drill Tool. Major Professor: Hazim El-Mounayri.

Previous works suggest that 80% to 90% of failures observed in the rotary machines are accounted to fatigue failure. And it is observed that cyclic stresses are more critical than steady stresses when the failure occurred is due to fatigue. One of the most expensive industries involving rotary machines is the Oil and Gas industry. The large drilling tools are used for oil extracts on-shore and off-shore. There are several forces that act on a drilling tool while operating below the earth surface. Those forces are namely pressure, bending moment and torque. The tool is designed from the baseline model of the former tool in Solidworks and Design Molder. Here load acting due to pressure and torque accounts for steady stress i.e., Mean Stress and loading acting due to bending moment account for fluctuating stress i.e., Alternating Stress. The loading and boundary conditions have been adapted from Halliburtons previous works for LWD drill tool to better estimate the size of the largest possible transducer. The fatigue analysis of static load cases is carried out in Ansys Mechanical Workbench 19.0 using static structural analysis. The simulation is run to obtain results for total deformation, equivalent stress, and user-defined results. The component is designed for infinite life to calculate the endurance limit. Shigley guideline and FKM guideline are compared as a part of a study to select the best possible approach in the current application. The width of the imaging pocket is varied from 1.25 inches to 2.0 inches to accommodate the largest possible transducer without compromising the structural integrity of the tool. The optimum design is chosen based on the stress life theory criteria namely Gerber theory and Goodman Theory.

1. INTRODUCTION

Oil well drilling is basically performed in making wells that broaden a few miles into the earth covering which could be ashore or beneath ocean bed on account of offshore boring [1]. There is a lot of unpredictability associated with drilling task which among many includes dealing with the fatigue stresses while optimizing the dimension changes from the baseline design. In the improvement or changes of the design, endurance is probably the most crucial property.

1.1 LWD Downhole Tool

Logging while drilling (LWD) is a technology of introducing well-logging tools. It goes into the borehole downhole. The whole arrangement is termed as the bottom hole assembly (BHA). LWD tools give the measurement related to geological formation downhole. The tool works as a system to transmit some or all measurements results to the surface. These results are called real-time data as the LWD system is still down-hole in the bore. And after the drill tool is pulled out of the bore down-hole the complete measured results can be downloaded. They are called Memory Data [2] [3].

Though these techniques are sometimes risky and expensive it has the advantage of being capable to measure the properties down-hole before drilling fluids reach deep below. Seldom well-bores prove to be difficult to measure with conventional wireline tools when the wells have highly deviated. These data are used so that the well-bore remains within the most productive portion of a reservoir, by guiding the placement of well. The LWD imaging technology helps deliver accurate models of the reservoir, optimum placement of well and reverses estimation for maximum oil extraction [2].

Originally MWD (measurement- while- drilling) technique was used to collect and record data downhole, LWD technique was an enhancement to the former technology

used to replace the wireline logging operation. Recently with the advancement in the downhole drilling technology, the LWD is a commonly used technology for drilling as well as formation evaluation [4].

To help gain better reservoir insights Logging-while-drilling (LWD) sensors record formation evaluation data, helping to take a timely decision and more precise placement of well [5]. A wide array of LWD sensors are offered by Halliburton Sperry Drilling which is engineered to provide specific reservoir data for geomechanical analysis, including petrophysical analysis and reservoir fluid characterization, enabling to enhance reservoir information and reduce the time of your drilling projects.

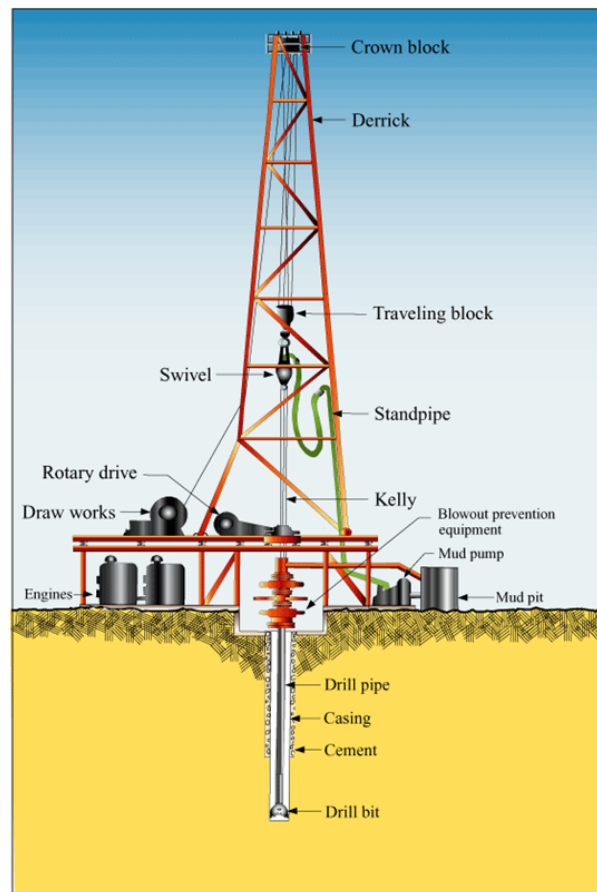


Fig. 1.1. Basic setup of BHA

Weight, bending, and torque on bit (real-time) measurements are provided by the tool to channelize energy from surface to the bit. Drilling parameters are optimized using these measurements which facilitates the optimization to achieve maximum performance and minimize wasted energy transfer and vibration. A full suite of vibration measurements is delivered the DrillDOC tool containing several sensors for providing the weight, bending moment and torque values and has a vibration sensor [5]. The full movement of the BHA is measured through all aspects of the drilling process which is ensured by this integration.

The sensor used for better imaging downhole is InSite AFR azimuthal focused resistivity sensor. It provides high-resolution structural and stratigraphic borehole images. This helps to precisely identify the fractures and pattern on the wall downhole and precisely provide the information of the permeability barriers and its location. It also provides information regards to borehole breakout, laterlog-type resistivity data, and at-bit resistivity (ABR) measurements. This was very difficult to determine with conventional logs. InSite AFR can provide high-resolution images, which are up to the standards of any wireline tool with imaging facility, and records fractures and formation while drilling [6].

The figure 1.2 below shows the application of the transducer in the LWD tool and Wireline tool. The transducer is closer to the wall in LWD so there are less attenuation and better signal transfer as compared to wireline tool where the transducer is far from the wall which leads to more attenuation and weaker signal strength [7].

1.2 Properties LWD Technology

Moderating risks by responding to changing drilling conditions continuously and rapidly identifying performance improvements to reduce downtime time and increase the rate of penetration (ROP) [5].

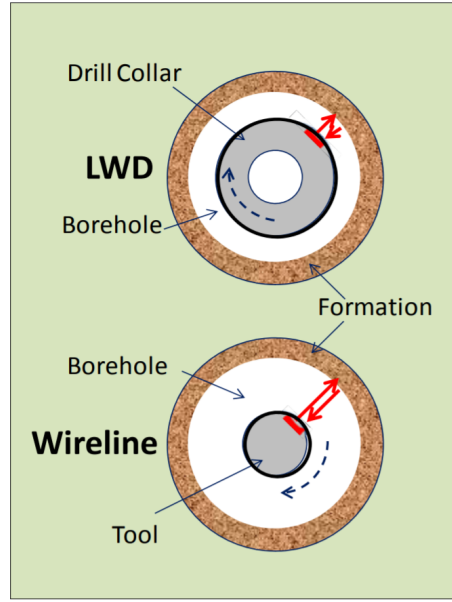


Fig. 1.2. Transducer application in the LWD tool and a Wire line tool

Recording what is beneath the subsurface can enable to recognize where hydrocarbons are situated in your store underground. Resistivity logging-while-drilling (LWD) tools assemble information to figure out which formations are loaded up with water (great transmitters of power) and those loaded up with hydrocarbons (poor transmitter of power). The resistivity logs and porosity measurements help in assessing water or oil immersion and assessing the producibility of formation. [3]

LWD resistivity tools offer various kinds of resistivity sensors to precisely distinguish varieties in resistivity around the borehole, from a couple of inches (centimeters) to several feet (meters) away. This enables to securely and certainly explore and geosteer through complex geologic structures while increasing exposure of the well to the most productive areas.

1.3 Acoustic Imaging

A single acoustic transducer is used both as the transducer and receiver, it functions as an acoustic imaging device. The transducer produces a pulse from the tool

to the bore wall. This acoustic pressure pulse propagates radially towards the bore wall. Once the signal is reflected the obtained images are interpreted to measure the distance from the wall and reflectivity. There are many factors which account for the limiting quality of the images obtained from the transducer. The mud and the diameter of the borehole (the distance of the transducer from the formation) account for the attenuation of the acoustic signal. Better image produced downhole helps better decision making in order to further steer the drill tool downhole. Greater the attenuation of the signal the poor result of the image which in turn leads to producing bad judgments. There are several ways to improve signal strength and reduce attenuation. One of them is by increasing the transducer size radially. The strength of the signal is directly proportional to the size of the radial cross-section of the transducer [8].

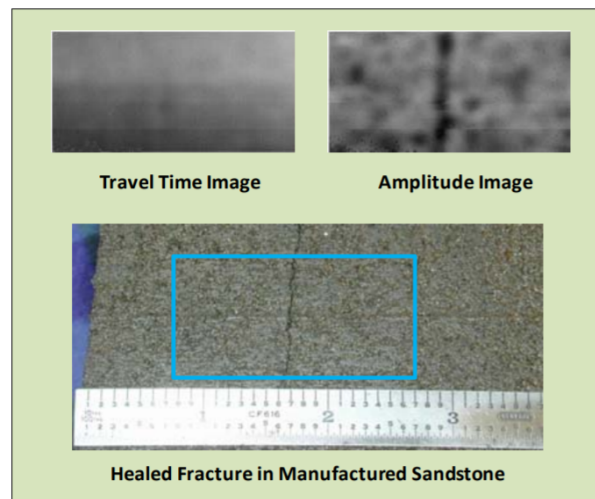


Fig. 1.3. Two ultrasonic images are obtained by mapping the measured travel time and attenuation

1.4 Transducer

A transducer is a round disk of ceramic expanding in thickness when a voltage is passed across it. When the acoustic energy produces a differential of pressure across the thickness, the ceramic produces the voltage. To prevent the signal propagating

from the back side a backing material is attached below the ceramic. The major concept in designing is gathering larger energy concentration in the smallest area possible, which is too idealistic to achieve. If it were not for the attenuation of the signal by the factors like mud, the design of the transducer would be much simpler. Several experiments were conducted in order to obtain optimum transducer size. According to the results, an increase in the diameter of the transducer reduces the attenuation produced by signal hitting the wall and reflecting. Moreover, it could be concluded from figure 1.4, that larger the diameter of the transducer the improved the imaging quality and lesser attenuation of the signal than the smaller diameters [8].

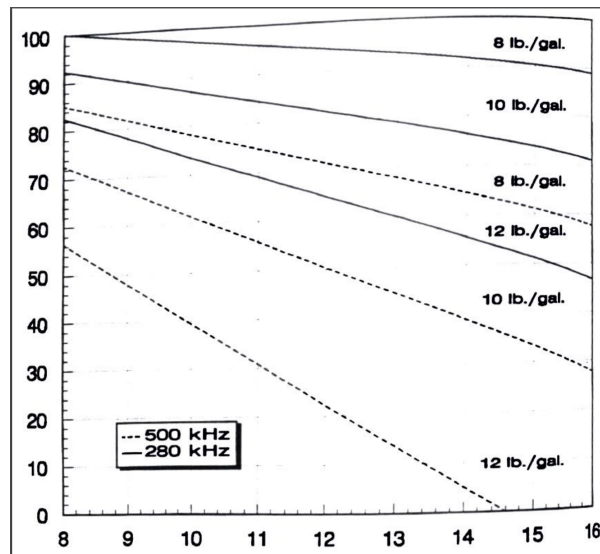


Fig. 1.4. Comparison of signal amplitude vs. borehole diameter

1.5 Project Scope and Layout

Design and fatigue analysis of an acoustic imaging section of LWD drill tool:

1. Literature research on fatigue failure and structural analysis of rotary machines observing cyclic load.

2. Experimental research on geometric design of the acoustic section of drill tool in order to accommodate 4 largest possible transducers placed radially opposite to each other along the central axis of the tool.
3. Material study of Nickel based alloy 718 for its application in drilling and calculating its endurance limit.
4. Analyzing the experimental results and optimizing the width of the imaging pocket using the study of stress theories and endurance limit calculations.
5. Submitting a report with respect to the guidelines of IUPUI and Purdue School of Engineering and Technology with systematic documentation of product developed with results and data gathered.

Endurance limit can be calculated by various methods like S-N diagram, Shigley-guideline, and FKM-guideline. For Inconel 718 the fatigue test data is not available through data points so guidelines are used to calculate the endurance limit. In this paper, two different approaches to be compared are Shigley and FKM guideline. The best of the two methods will be selected to perform fatigue failure analysis. Based on the analysis of 16 different design points, the feasible designs are nominated. Out of the feasible designs, the optimum design is suggested based on the requirement.

1.6 Problem Statement

Design and Fatigue analysis of an LWD drill tool:

- Design Variables - The width of the imaging pocket on the drill tool is varied from 1.25 inch to 2.0 inch and the radius of the fillet is varied from 0.08 inch to 0.1 inches.
- Design constraint - The alternating stress should be less than 50,000 Ksi; The Gerber stress theorys user-defined value should be less than 1; The Goodman stress theorys user-defined value should be less than 1.

- Result analyzation - To fit the largest possible transducer with reducing the structural integrity of the tool. A drilling tool has a lot of forces acting on it which results in fatigue failure of the tool. This project concentrates on imaging section of the whole LWD drill tool.

1.7 Organisation of Report

The report is divided into five chapters. A preface and introduction to this thesis are given in the first chapter, followed by a chapter briefly describing drilling operations and the applicability of LWD and MWD tools. The second chapter discusses the previous works that are done in fatigue analysis and rotary machines. Then the third chapter discusses the load applied on the drill tool which is generally described with emphases on some key parameters such as pressure, bending moment and torque in a medium. The fourth chapter described how the experiments were carried out, the FEA setup and procedure of the prototype tool. In the fifth chapter, the results and analysis of the design and fatigue analysis are presented.

2. LITERATURE REVIEW

A lot of research is conducted in the fatigue analysis of different types of equipment which are used in drilling purposes. These drilling tools are dynamic in nature as to drilling different types of ground terrain. While doing so a lot of stress is generated and that ultimately leads to a lot of fatigue. Fatigue, in general, is defined as stress that is developed due to repetitive applied loads which lead to localized stress and structural damage [9]. Such kinds of failure can be harmful to the tool and can cause damage to the work process and environment. Thus, tackling failure is an important department in any mechanical process as it keeps the process safe. An analysis is the first step to eradicate any failure occurrence and analysis is thus a major part of this study. Failure analysis is defined as the process of overcoming localized stress which leads to failure and can be done using computational methods, physical methods, and laboratory methods. There are many reasons which lead to failure which can be found out by proper analysis, these can be design flaws, material problems, improper usage of standards, etc. Design adjustments can be done to keep the fatigue failure caused by localized stress away, it also helps to reduce manufacturing cost, reduce material cost, allows better efficient models to incorporate better results.

2.1 Studies on Turbine Blade

Recently a research was conducted by scientists of China Aero-Polytechnology Establishment on turbine blades in the air cycle machine. The frequent damage in air cycle machine MA60 of the aircraft was the driving reason for them to conducting a fatigue life analysis. In their analysis, centrifugal force and aerodynamic force were the two loads causing equipment failure. After computing the boundary condition, which is equivalent to real boundary conditions, two result analysis are carried out

which are the fluid simulation and static force simulation. In Fluid simulation analysis contours of static pressure and absolute pressure were examined and in static force simulation fluid pressure, Von-mises stress, Max. Principal stress, Min. Principal stress and total deformation were examined. Further through Goodmans theory life of the blade was calculated [10].

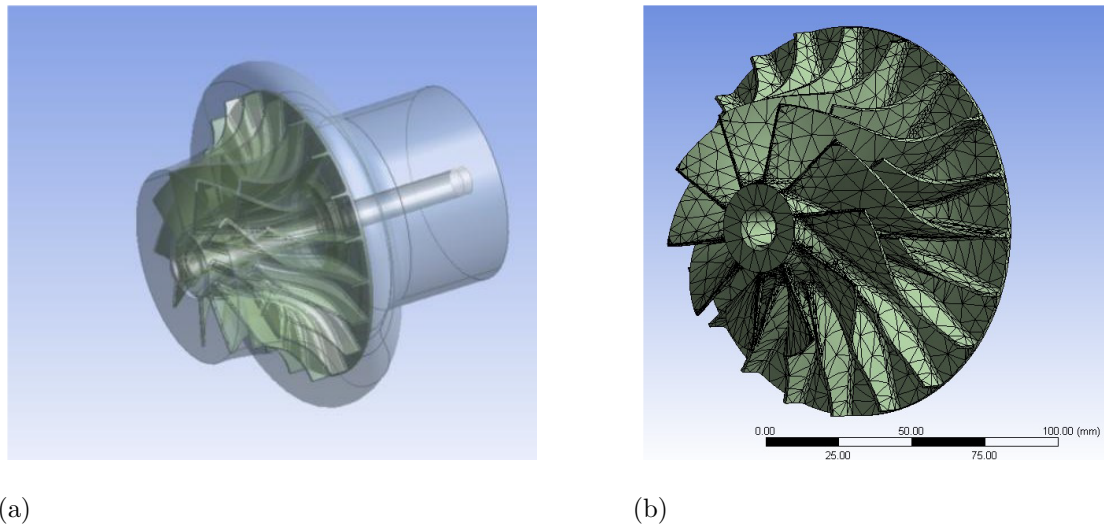


Fig. 2.1. CAD model and FEA model of a turbine blade

2.2 Failure Analysis of a Drill Pipe

Further, similar research was conducted in Iran on Failure analysis of a drill pipe. It discusses the impact of loads and stresses which in turn raises the probability of failure by causing a reduction in fatigue strength. The primary form of loads and stresses considered in this research was vibration and its impact. The stress concentration in drill pipe is divided into four groups surface irregularities, upset area, corrosion pitting, and threaded connections. With the help of Ansys Mechanical Workbench, stress state was analyzed and found the weakest position of the drill pipe. As shown in the figure below upset areas, threaded connections and holes are some of the critical fatigue regions of the drill pipe. And with the analyses it was found that factors that

have an impact on the number of induced stresses and vibrations are weight on bit (W.O.B), rotating speed of drill string and bit (RPM), flow rate (GPM), pressure, type and weight of mud, formation, rate of penetration (R.O.P), inclination(Inc), dogleg severity(DLS), hole size, bit type, bottom hole assembly(BHA)arrangement , mass imbalance, stabilizer blades and using mud motors [11].

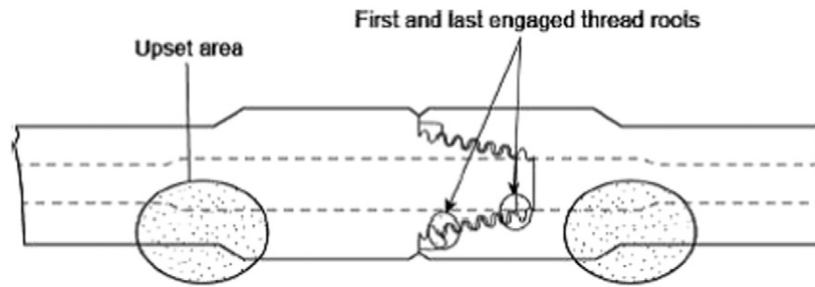


Fig. 2.2. Critical fatigue regions of the drill stem and connection

In another research that was conducted in China, fatigue failure analysis of drilling tools was performed. It primarily considered the impact of axial stress and bending stress to ensure that the tool withstands the alternating load in the drilling direction. In the result computation, the stresses were examined to analyze stress concentration which was found near the corner of the shoulder. After applying a variable load, S-N model was used to calculate fatigue life. The results showed that under high load, the tool observed low fatigue life at stress concentration point. The research concludes that the main cause of failure is fatigue damage due to large axial force, long corrosion time and high temperature [12].

In a research conducted in 2009 need of a high-resolution LWD resistivity imaging tool was discussed. It describes the requirement of a technology to log data and store the image of surface downhole. The results of measurements are calibrated resistivity images with resolution limits of 0.5-1 inch which depend upon the size of the transducer. It also discusses the operating principle of the transducer and the tool, their key design parameter and the environmental parameters that influence the

result. An LWD drill tool, the AFR, has been introduced for solving a variety of geological, petrophysical and operational problems in conductive boreholes [6].

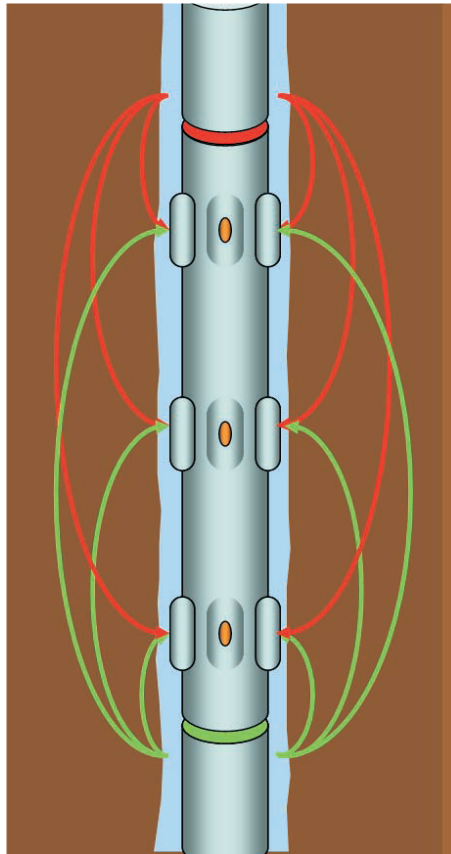


Fig. 2.3. AFR model for the at-bit measurement

2.3 Fluctuating Stress Studies of a Dove-Tail Joint

In another research, conducted by Kaliyaperumal Anandavel, Raghu V. Prakash and Antonio Davis, the effect of preloading on stresses, slip levels and contact traction at dovetail blade-disc interface of an aero-engine using FEA. The effect of pre-stress on a strip of specimen analyzed using structural analysis. The preloading of specimen gives an impact on the cyclic stress amplitude. The model is analyzed with boundary conditions and assuming cyclic symmetric loading conditions. The results are taken over 10 load cases and angular velocity [13].

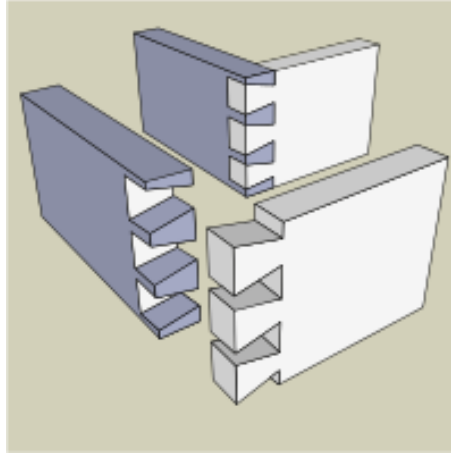


Fig. 2.4. Dovetail Joint

2.4 Optimization and Fatigue Analysis of Differential

Previously an experiment has been conducted of optimization and fatigue analysis of an automotive component. In order to perform fatigue analysis, two methods were used one being quasi-static simulation with independent static cases and other being transient analysis. The fatigue stress observed in the component was evaluated using the stress-life approach. Later the two approaches are compared for the stress analysis. Thus, in this study, the new differential design is evaluated for fatigue stresses using a stress-life approach [14].

2.5 Previous Analysis of Baseline Tool

The drill tool in this project of 6.75inch diameter was developed from a baseline of 4.75inch diameter. Previous an analysis was carried out on the baseline model with the three loads being applied on it. These loads were 30,000 psi of pressure, 35,000 lbf.ft of torque and a bending moment of $15^{\circ}/100ft$. The results were analyzed for studying stress accumulation in the drill tool.

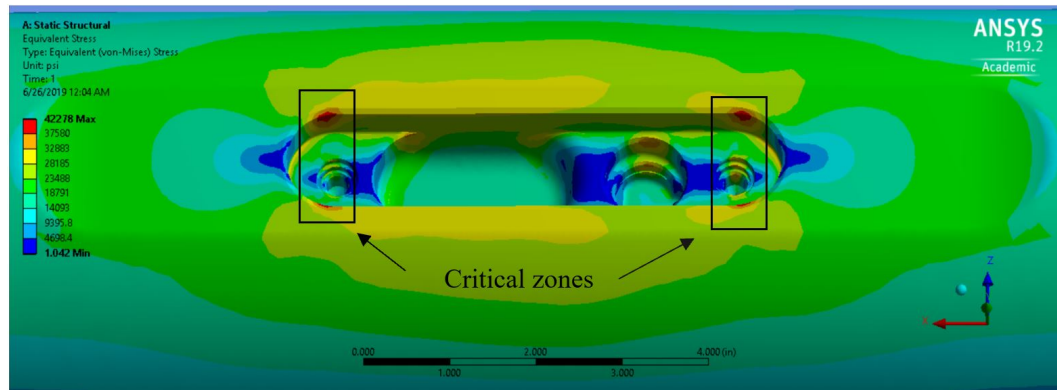


Fig. 2.5. Equivalent stress for rotating bending moment applied on the baseline tool

From the figure above it is understood that stress accumulation tends to occur in an undesirable zone. Thus, while developing the design of 6.75inch diameter, observations from the above analysis are carefully considered.

2.6 Summary of Previous Works

With the above research, it is concluded that since an LWD tool is a downhole drill tool that faces rotational and cyclic loading and unloading it is most likely to collapse under fatigue failure. Studies show that the impact of transducer size on the results of the downhole image of the wall surface is significant. Larger the distance of transducer from the surface, greater the attenuation of the transmitting signal. And to accommodate geometry changes in a drill tool to fit in a larger transducer it is required to perform fatigue analysis to ensure that the design optimized for the larger transducer does not reduce the structural strength and integrity of the tool. Thus, this study will be performed for an endurance limit calculation to compute allowable alternate stress for the tool. Further stress-based life theory like Goodman and Gerber theory will be used to confirm the safety of the tool from failure.

3. METHODOLOGY

The following figure 3.1 shows the workflow for the analysis of fatigue stresses in the drill tool. First, the component is designed from the baseline of the former drill tool of 4.75inch diameter using CAD software. Next, the FEA analysis is done using Ansys Mechanical Workbench 19.0 which requires the geometry model of the component, the material database of the chosen material to be used for the analysis and the loading parameters such as the bending moment, pressure and torque are the forces acting on the component. Further, the fatigue stresses are identified and analyzed from the FEA analysis solution. The endurance strength with the endurance correction factors are considered to get the feasible set of design points and finally, the solution of the optimum design point is found out with the help of Goodman, Gerber and FKM theory.

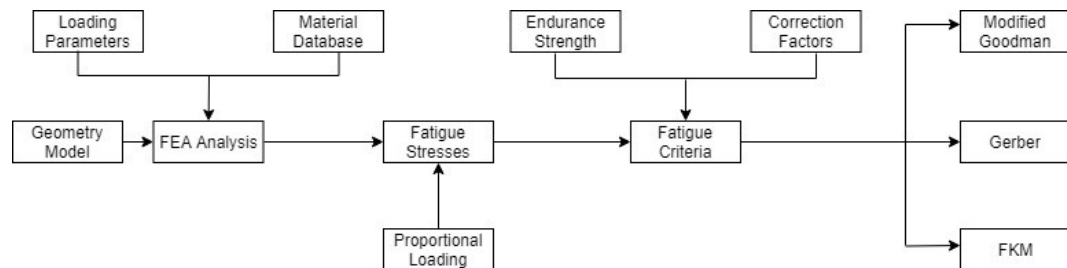


Fig. 3.1. Workflow of the project

3.1 The CAD Model

The prototype of the imaging section of the LWD drill tool consists is discussed in this section. The tool is re-designed by keeping the previous member of the LWD tool (4.75 in diameter) family as the base for design features. The geometry consists of a

feature to hold the electronics like acoustic transducer and receiver. It has two holes holding the bolts for the assembly. The geometric dimensions of the tool are 6.75-inch major diameter and 2 inches of borehole diameter. The cross section of the tool is shown below in the figure. The geometry of the tool and the application of loading conditions are inspired by the project assigned by Halliburton as an internship task.

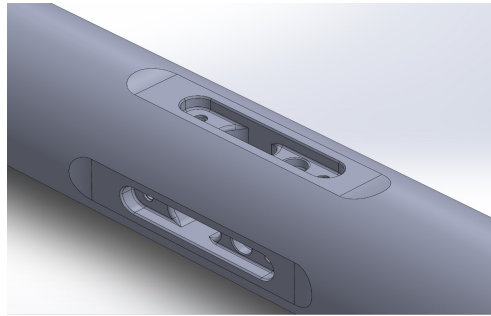


Fig. 3.2. Isometric View of imaging pocket

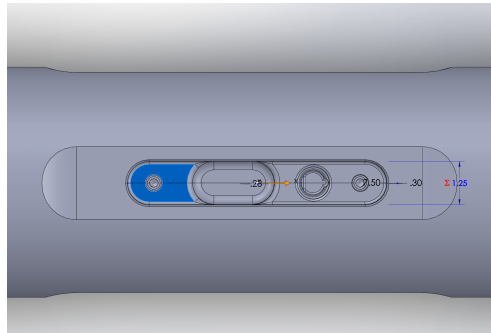


Fig. 3.3. Top View of imaging pocket

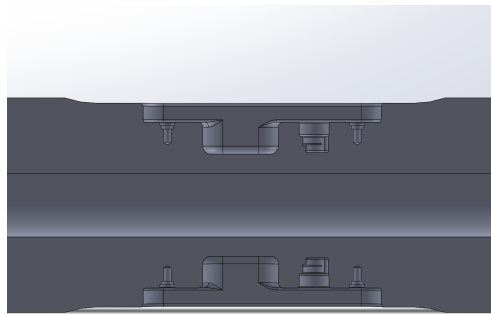


Fig. 3.4. Cross-sectional view along the XZ plane

The objective is to accommodate the four largest possible transducers placed radially along the central axis without compromising its mechanical strength. In order to achieve the above objective, the width of the imaging pocket is varied from 1.25 inch to 2.0 inch. Along with the width, the other parameter which is varied to reduce stress concentration is the fillet of the imaging pocket. The forces acting on the tool which leads to fatigue failure are pressure, bending moment and torque.

3.2 Types of Load Applied

There are three major types of load on the drill tool: Under the drilling action downhole, the tool faces different types of forces like pressure, bending moment and torque. These forces result in the tension and compression of the imaging pocket.

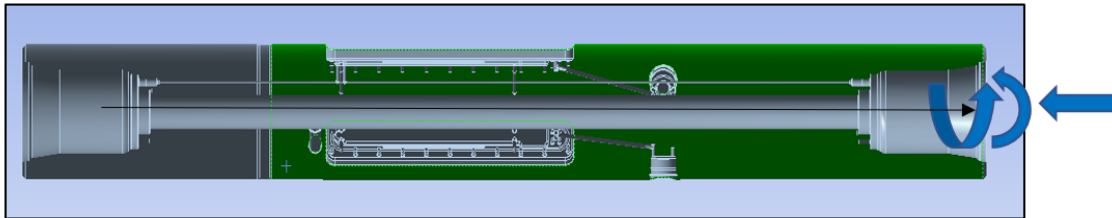


Fig. 3.5. Loads acting on the drill tool

Pressure load: The pressure load acts on the whole drill tool along with the imaging pocket. The pressure applied is 30,000 psi in magnitude and the direction of the load is normal towards the surface of the drill tool and the axial center of the drill tool.

Bending Moment: As shown in figure 3.7 below, the magnitude of bending moment is 150/100 ft. This means for every 100 feet displacement; the drill tool can be steered by 15 degrees. The bending moment acts on three directions but is restricted to move axially in the x-direction and is free to move in the y-z plane. The flex tool is used to calculate the appropriate face rotation for the 15 degrees of the bend. Also,

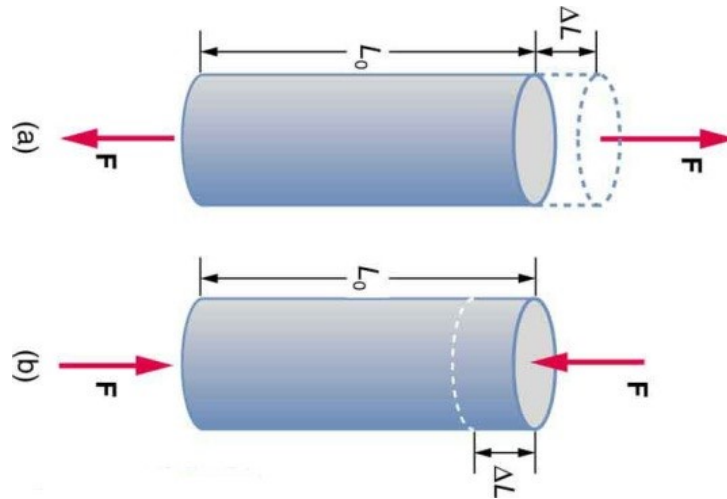


Fig. 3.6. Tension and Compression on the tool

the value of face rotation can be obtained by the following equation: Assuming the length of the drill tool as 50 in (4.17 ft), solving for X gives,

$$\frac{15}{100ft} = \frac{X}{4.17ft} = 0.625ft/degree \quad (3.1)$$

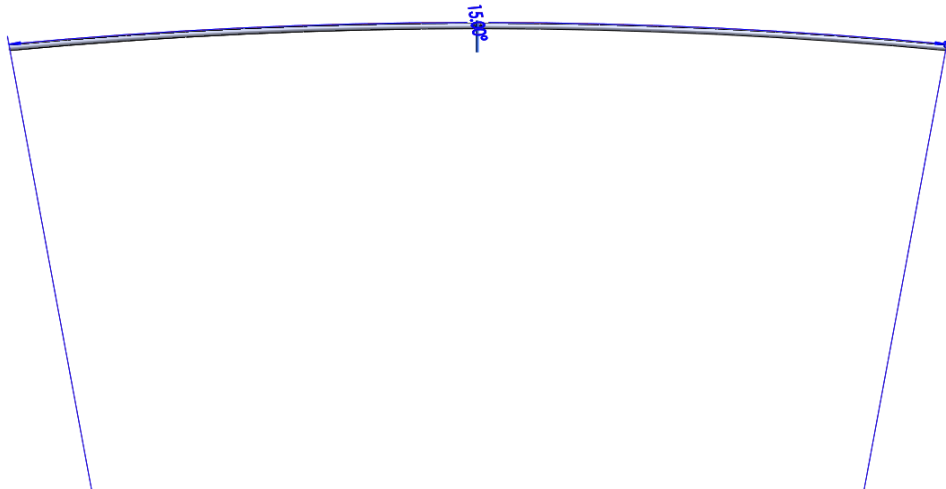


Fig. 3.7. Flex for deflection of the drill tool

Torque: The torque acts on the end faces through the central axis of the drill tool. The magnitude of the torque is 35,000 lb.ft.

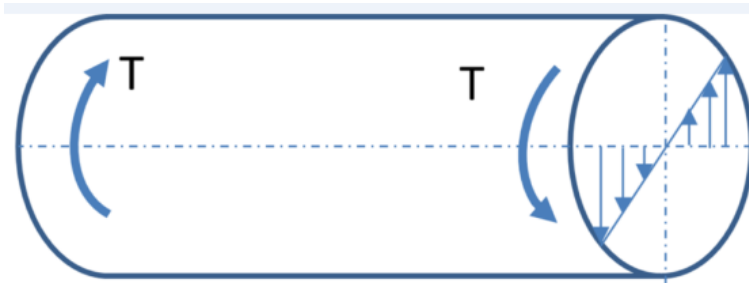


Fig. 3.8. Rotational Torque acting on the tool

3.3 Material Properties

Inconel alloy 718 is a high-strength, vacuum-melted corrosion-resistant nickel chromium material used at $-423^{\circ}F$ to $1300^{\circ}F$. The age-hardenable alloy can be promptly prototyped even into complex parts. Its welding qualities, particularly its protection from post-weld cracking and strain-age cracking, are exceptional. It is also readily formable. Depending on the choice of temperature it has good oxidation resistance up to $1300^{\circ}F$. The ease and economy with which Inconel alloy 718 can be manufactured, joined with good tensile, fatigue, creep, and rupture strength, have brought about its utilization in a wide scope of applications. These properties of Inconel make it an ideal fit for the drilling application. The table 3.1 below shows the composition of elements in Inconel alloy 718 [15].

Physical Properties:

- Tensile Strength: 150,000 psi
- Ultimate tensile strength: 180,000 psi
- Density: 0.296 lb/in^3
- Melting Range: 2200-2450 F / 1210-1344 C

Table 3.1.
Composition of metals in Inconel 718

Element	Minimum	Maximum
Carbon	–	0.08
Manganese	–	0.35
Silicon	–	0.35
Phosphorus	–	0.015
Sulphur	–	0.015
Nickel + Cobalt	50.0	55.0
Chromium	17.0	21.0
Cobalt	–	1.00
Iron	Balance	Balance
Aluminium	0.35	0.80
Molybdenum	2.80	3.30
Titanium	0.65	1.15
Boron	0.001	0.006
Copper	–	0.15
Cb + Ta	4.75	5.50

3.4 Design of an LWD Drill Tool

Design improvement is satisfying the project requirements along with the process of finding suitable design parameters. Engineers mostly use the design of experiments (DOE), measurements, and optimization methods to assess trade-offs and decide the best plan to improve the design. Designing of a tool can involve various design objectives like minimum weight under allowable stress, minimum compression over a particular area, to minimize or maximize one or more dimension avoiding stress accumulation, to optimize feature dimension to avoid weakening of the structure [16].

Table 3.2.
Mechanical properties of Inconel at different temperatures

Temperature, $^{\circ}F$	Young's Modulus	Torsional Modulus	Poisson' Ratio
100	28.8	11.2	0.291
200	28.4	11.0	0.288
300	28.0	10.9	0.280
400	27.6	10.8	0.280
500	27.1	10.6	0.275
600	26.7	10.5	0.272
700	26.2	10.3	0.273
800	25.8	10.1	0.271
900	25.3	9.9	0.272
1000	24.8	9.7	0.271

Characteristic of design problem:

- While designing it is to be considered that there exists more than one solution and the best-suited solution needs to be determined.
- There are multiple objectives defined which are measured on the basis of how well they are accomplished.
- Different kinds of constraints are imposed which could be hard or soft depending upon the expected outcome.

There could exist many variables which influence and impact the measurable performance. It can either improve or worsen the performance and violate the constraints. The problem statement of this project has only two variables which makes it relatively simpler. Thus, designing can be defined as a problem where there are certain parameters, also can be design variables, defined to attain best measurable performance while satisfying the specified constraints.

Formulation of the design problem can involve the following steps: [16]

1. State design objectives,
2. State design constraints,
3. Identify design variables.
4. Provide a feasible set of solution

Objective is to accommodate 4 largest possible transducers placed radially opposite to each other along the central axis of the tool.

Design Variable is also called a control variable as it is a decision maker and has an impact on the solution of the design problem. Each combination of design variables represents a unique design [16]. For this project, the width of the imaging pocket on drill tool is varied from 1.25 inch to 2.0 inch and the radius of the fillet is varied from 0.08inch to 0.1inch.

Design constraint are:

1. The alternating stress should be less than 50,000 psi (endurance limit)
2. The Gerber stress theorys user-defined value should be less than 1.
3. The Goodman stress theorys user-defined value should be less than 1.

The feasible set of design points are provided in chapter 4. And the optimum design suggestion is discussed in the results section following the graphical method of solution.

3.5 Fatigue Life

It is evaluated that somewhere in the range of 50 to 90 percent of product failures are brought about by fatigue and reliant on this fact, fatigue analysis ought to be a part of all product enhancement.

While testing the properties of materials very often a condition arises where the load applied, and stress generated vary depending on time. The types of load which result in similar stresses are variable, repeated and alternating stress. Fatigue is defined as loss of strength of material by repeatedly applied loads over a definite or indefinite number of cycles. Especially when the material is under cyclic loading (alternating stress) it results in localized stress in critical zones. Loading and unloading of forces result in fatigue in the material. And often components fail under the fatigue caused by the alternating stresses. On analysis, it is known that the actual maximum stress noted was far below the ultimate strength of the component material. But what is typical was the stress that was repeated a large number of times. Thus, failure caused under such situations is called fatigue failure. Fatigue failure normally occurs in the form of brittle fracture even when stresses are well below the static strength of the materials, it is highly dangerous when such failure occurs [17] [18].

The fatigue analysis of the drill tool was performed using ANSYS workbench mechanical. As the S-N curve information of the material used is not accessible another methodology should be adopted for analyzing the fatigue in the drill tool. The fatigue life of a part relies upon mean and alternating stress that part encounters. The pressure load due to torque and pressure are considered as stresses acting as mean stress on the drill tool. As we know fatigue is a time-dependent property so a fluctuating load is required to provide for alternating stress which applied in the form of bending moment. Out of the three possible methods available for time-varying load which are static analysis, transient analysis, and modal based transient analysis, the static structural approach is adopted in this paper [14].

In the world of material science, engineers widely follow three methods to predict fatigue life using materials mechanical properties. Those methods are the stress-life method, the strain-life method, and the linear-elastic fracture mechanics method. The situations which exceed more than 10^4 life cycles are given more importance [19].

3.5.1 Stress-Life Method

The approach in this paper follows the stress-life method to solve for fatigue limit. The stress-life method is used specifically where a large number of life cycles are involved. It is also called Infinite life design. Wherever the stresses observed are elastic it is recommended to use the stress-life method. It is based on the endurance/fatigue limit. It was the first approach used in an attempt to understand and measure metal fatigue. The mechanical properties of the material are modified for surface conditions, like notches, and loading conditions are computed. This method does work well where the applied stress has a substantial elastic component. In the laboratory, the material, usually shaft, is exposed to repetitive stress while counting cycles to failure. As it starts to rotate the alternating stress starts to fluctuate between the same magnitude of different direction i.e., tension and compression. This is known as a completely reversed stress cycle. Depending upon the nature of material and failure, maximum principal stress is recommended for brittle failure and Von-mises stress is recommended for ductile materials. The Goodman stress theory is used to obtain the equivalent alternating stress with zero mean stress [20].

3.5.2 Endurance Limit Calculation

Endurance limit is the expression used to describe a property of materials which define the failure point. The maximum alternating stress that can be applied to the material without causing fatigue failure is known as Endurance limit. Endurance limit, fatigue strength and fatigue limit are all quantities describing a similar property of the material. In other words, endurance limit, S_e , is the stress value below which failure never occurs even for a large or infinite number of cycles. The determination of endurance limit is important for material which is subjected to high-cycle fatigue to ensure that the stress produced in the element is always below the endurance limit of the material. Usually, strain testing is not preferred when the endurance limit is being calculated. When endurance tests of some parts are not available through the

S-N diagram, approximations are made by using Shigley - guideline or FKM guideline to the endurance limit. The value of endurance limit largely depends on the surface quality of the material. As a notched material has a significantly lower value of the endurance limit [21].

Endurance Limit - Shigley guideline: Industries involving high cycle fatigue largely follow Shigley - guideline for calculating endurance limit. The Shigley guideline is predominantly based on test data recorded earlier than the 60s. Recently in 2014, a new revision was proposed for some of the endurance limit modifying factors and rest remained unchanged. Based on the two guidelines from 1983 and 2014, the endurance limit is calculated and compared for better decision making. For steels, the endurance limit is calculated and compared for better decision making. For steels, the endurance

$$\text{limit is estimated as } S'_e = C_E * S_{ut} S'_e = \begin{cases} 0.5 * S_{ut} & S_{ut} \leq 200 \text{ksi} \\ 100 \text{ksi} & S_{ut} > 200 \text{ksi} \end{cases} \quad (3.2)$$

Thus $S'_e = 90,000 \text{psi}$

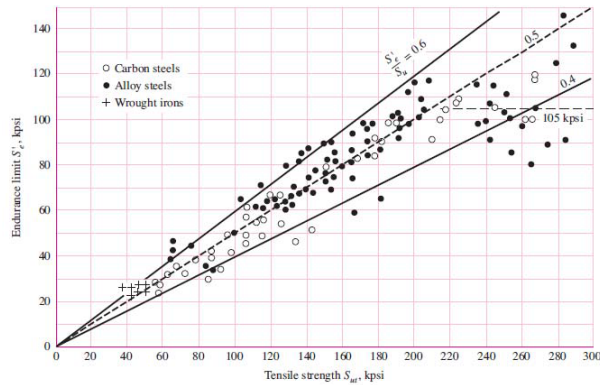


Fig. 3.9. Data from Fatigue Design Handbook, SAE, 1968

S'_e is the endurance limit of rotating-beam specimen used in the laboratory and is prepared very carefully and tested under monitored-controlled conditions. It is not realistic that the endurance limit of a mechanical component will match the values obtained in the laboratory. Factors like material composition, manufacturing methods, environmental conditions, and design dimension affect that value [22] [21].

Shigley-guideline identifies and quantifies those factors as following:

$$S_e = k_a * k_b * k_c * k_d * k_e * k_f * S'_e \quad (3.3)$$

Where k_a : surface condition modification factor

k_b : size modification factor

k_c : load modification factor

k_d : temperature modification factor

k_e : reliability factor

k_f : miscellaneous-effects modification factor

S'_e : rotary-beam test specimen endurance limit

S_e : endurance limit at the critical location of the geometry

C_E : Endurance limit factor for materials

1. Surface factor, k_a :

The equation of the surface correction factor is given by the following equation:

$$k_a = a * (S_{ut})^b \quad (3.4)$$

where S_{ut} is the ultimate tensile strength and a and b are found from table 3.3.

Table 3.3.
Surface Correction Co-efficient 'a' and 'b'

Surface finish	Factor 'a' (S_{ut} in ksi)	Factor 'b'
Ground	1.34	-0.085
Machined or cold-drawn	2.70	-0.265
Hot-rolled	14.4	-0.718
As - forged	39.9	-0.995

Thus, for Inconel 718 (machined surface), we know $S_{ut} = 180,000$ psi, $a = 2.70$ and $b = (-0.265)$ $k_a = 0.681$

2. Size factor, k_b :

The size factor is calculated with the help of 133 sets of data points [21]. The equation is expressed as following for bending and torsion

1983 Guideline:

$$k_b = \begin{cases} 1 & d \leq 0.3in \\ 0.869d^{-0.097} & 0.3 \leq d \leq 10in \end{cases} \quad (3.5)$$

For $d = 6.75$ in, $k_b = 0.722$ (1983);

2014 Guideline:

$$k_b = \begin{cases} 0.91d^{-0.157} & 2 \leq d \leq 10in \\ (d/0.3)^{-0.107} = (0.879d)^{-0.107} & 0.11 \leq d \leq 2in \end{cases} \quad (3.6)$$

For axial loading, there is no size effect, $k_b = 1$. For $d = 6.75$ in, $k_b = 0.674$ (2014).

3. Load modification factor, k_c :

For bending load applied k_c is always unity i.e., $k_c = 1$.

4. Temperature modification factor, k_d :

In 1983 edition, the equation for correction factor is given as follows, when $T_F \leq 842^\circ F$ $k_d = 1$ The revised edition (2014) equation is given as follows, when $70 \leq T^\circ F \leq 1000^\circ F$

$$k_d = 0.975 + 0.432(10^{-3})T_F - 0.115(10^{-5})T_F^2 + 0.104(10^{-8})T_F^3 - 0.595(10^{-12})T_F^4 \quad (3.7)$$

For $T = 392^\circ F$, $k_d = 1.016$

5. Reliability factor, k_e :

There is no recommendation provided in Shigley - guideline for reliability. Its dependent on the users decision. For simplification, the reliability factor is used for 97.5% .Thus, from the table below $k_e = 0.843$.

Table 3.4.
Reliability Factor as given in Shigley book of Machine Design

Reliability	k_e
0.5	1.000
0.90	0.897
0.95	0.868
0.975	0.843
0.99	0.814
0.999	0.753
0.9999	0.702
0.99999	0.659

6. Miscellaneous factor, k_f :

Since the Inconel shaft is not sensitive to a notch, the miscellaneous factor is unity i.e., $k_f = 1$

Thus, the endurance calculated using the guidelines of 1983 and 2014 revision is as follow,

For 1983 edition, $S_e = 0.681 * 0.722 * 1 * 1 * 0.843 * 1 = 37,296$ psi

For 2014 edition, $S_e = 0.681 * 0.674 * 1 * 1.016 * 0.843 * 1 = 35,379$ psi

FKM guidelines:

The FKM guideline was initially developed in Germany in 1994 and are updated periodically since then. This guideline was a collaboration between an expert group Strength of Components of the Forschungskuratorium Maschinenbau (FKM) with

financial support by BMW, Arbeitsgemeinschaft industrieller Forschungsvereinigungen, Otto von Guericke, and Forschungskuratorium Maschinenbau, etc. FKM guidelines are well accepted in the US manufacturing industries and widely used in German industries. Moreover, these guidelines are widely adopted by commercial software companies like KissSoft, ANSYS, ADIANA, AutoFENA 3D and many more [23]. The modification factor for calculating the corrected endurance limit is as follows:

$$S_e = C_E * C_T * C_R * C_q * C_D * C_s * S_{ut} \quad (3.8)$$

Where,

S_e the endurance limit at the critical location of the specimen with consideration of geometry and condition in use.

S_e the endurance limit obtained from the rotating beam test.

C_E Endurance limit factor for materials

C_T Temperature correction factor

C_R Reliability factor

C_q Roughness correction factor

C_D Size correction factor

C_s Surface treatment/condition correction factor

For Inconel 718 and the geometry shown in figure 3.1-3.3:

$$S_e = CE * S_{ut} \quad (3.9)$$

Therefore, for Inconel 718:

$$S_e = 0.45 * 180,000 = 81,000 \text{ psi}$$

Table 3.5.
Endurance Limit factor

Material Type	$C_{e,E}$
Case hardening steel	0.40
Stainless Steel	0.40
Forging steel	0.40
Steel casting	0.34
Other types of steel	0.45
Ductile iron	0.34
Malleable cast iron	0.30
Gray cast iron	0.30
Wrought aluminum alloys	0.30
Cast aluminum alloys	0.30

1. Temperature correction factor:

For $T > 100^\circ C$,

$$C_T = 1 - 1.4 * 10^{-3}(T - 100), \quad (3.10)$$

At $T = 200^\circ C$, $C_T = 0.85384$

2. Reliability factor:

Note: FKM-Guideline specifies that the ultimate tensile strength of a component for material should be based on the probability of a 97.5% survival rate i.e., $C_R = 0.843$.

Table 3.6 provides values for reliability factor at assumption of different percentage of reliability of the specimen.

Table 3.6.
Reliability correction factor (FKM guideline)

Reliability	C_R
0.5	1.000
0.90	0.897
0.95	0.868
0.975	0.843
0.99	0.814
0.999	0.753
0.9999	0.702
0.99999	0.659

3. Size Correction Factor:

For the element shown in the following table 3.7:

After referring relevant literature material, it is determined that Inconel 718 falls under steel, quenched, and tempered category [24].

Now, for steel, quenched, and tempered from the table:

$$C_D = 1.0 \text{ for } d_{eff} \leq d_{eff,min} \quad (3.11)$$

$$C_D = \frac{[1 - 0.7686 * a_d * \log(d_{eff}/7.5mm)]}{[1 - 0.7686 * a_d * \log(d_{eff,min}/7.5mm)]} \text{ for } d_{eff} > d_{eff,min} \quad (3.12)$$

Calculation of the effective diameter d_{eff} (Adopted from FKM-Guideline):

For the specimen shown in figure 3.1-3.33, the cross-section suggests

$$s = \frac{(O.D - I.D.)}{2} = 2.375in = 60.325mm \quad (3.13)$$

Table 3.7.
Size Correction Factor (FKM guideline)

Material Type	$d_{eff,min}$ in mm	a_d	Case of d_{eff}
Plain carbon steel	40	0.15	Case 2
Fine-grained steel	70	0.2	Case 2
Steel, quenched and tempered	16	0.3	Case 2
Steel, normalized	16	0.5	Case 2
Steel, case hardened	16	0.5	Case 1
Nitriding steel, quenched and tempered	40	0.25	Case 1
Forging steel, quenched, and tempered	250	0.2	Case 1
Forging steel, normalized	250	0.2	Case 1
Steel casting	100	0.15	Case 2
Steel casting, quenched and tempered	200	0.15	Case 1
Ductile iron	60	0.15	Case 1
Malleable iron	15	0.15	Case 1

(Figure 3.10) Thus, $d_{eff} = 60.325$ mm and $d_{eff,min} = 16$ mm, $d_{eff} > d_{eff,min}$.
Also, $a_d = 0.3$.

Accordingly, after all the substitution of coefficients with respect to the specimen, the value of the size correction factor is:

$$C_D = [1 - 0.7686 * 0.3 * \log(60.325/7.5)] / [1 - 0.7686 * 0.3 * \log(16/7.5)]$$

$$C_D = 0.856187.$$

4. Roughness correction factor:

According to FKM-Guideline, the roughness correction factors for stresses developed in the rotating element is obtained from following equation:

$$C_q = 1 - a_R * \log(Rz) * \log(2 * S_{t,u} / S_{t,u,min}) \quad (3.14)$$




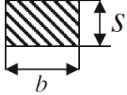
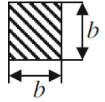
Cross section	d_{eff} Case 1	d_{eff} Case 2
Solid rod with round cross section	d	d
		
Tubular rod with round cross section	$2s$	s
		
Infinitely wide thin wall (tubes with large inner diameter)	$2s$	s
		
Solid rod with rectangular cross section	$\frac{2bs}{b+s}$	s
		
Solid rod with square cross section	b	b
		

Fig. 3.10. Effective diameter for different cases

For machined surface assume roughness value $R_z = 125 \text{ m}$ and $a_R=0.22$. Thus, after all the substitutions, $C_q = 0.7942$.

Table 3.8.

Material Type	a_R	$S_{t,u,min}$
Steel	0.22	400
Steel Castings	0.20	400
Ductile iron	0.16	400
Malleable cast iron	0.12	350
Gray cast iron	0.06	100
Wrought aluminum alloys	0.22	133
Cast aluminum alloys	0.20	133

5. Surface correction factor:

For the Inconel shaft, the surface correction factor is $C_s = 1.1$, as its surface treatment is shot peened.

The surface correction factor for the various components is as follows: Therefore, the corrected endurance limit after substitution of all the factors is as follows:

$$S_e = (0.45 * 0.85384 * 0.843 * 0.794264 * 0.856187 * 1.15 * 180,000) = 45,595.3 \text{ psi.}$$

Comparison of Shigley vs FKM guideline:

On comparing the endurance limit obtained by three different guidelines, we can conclude from table 3.8 FKM guideline allows more alternating stress as endurance limit than the Shigley both the edition.

Thus, after careful comparison, it is concluded that the FKM approach will be se-

Table 3.9.
Comparison of Guidelines for Endurance Limit

Guideline	Shigley (1983)	Shigley (2014)	FKM
Endurance limit, S'_e (psi)	37,292	37,292	45,595.3

Surface treatment	Unnotched components	Notched components
<i>Steel</i>		
Chemo-thermal treatment		
<i>Nitriding</i> depth of case 0.1–0.4 mm, surface hardness 655–926 HB	1.10–1.15 (1.15–1.25)	1.30–2.00 (1.90–3.00)
<i>Case hardening</i> depth of case 0.2–0.8 mm, surface hardness 628–701 HB	1.10–1.50 (1.20–2.00)	1.20–2.00 (1.50–2.50)
<i>Carbo-nitriding</i> depth of case 0.2–0.8 mm, surface hardness 628–701 HB	(1.80)	
Mechanical treatment		
Cold rolling	1.10–1.25 (1.20–1.40)	1.30–1.80 (1.50–2.20)
Shot peening	1.10–1.20 (1.10–1.30)	1.10–1.50 (1.40–2.50)
Thermal treatment		
<i>Inductive hardening, flame hardening</i> depth of case 0.9–1.5 mm, surface hardness 495–722 HB	1.20–1.50 (1.30–1.60)	1.50–2.50 (1.60–2.8)
<i>Cast iron materials</i>		
Nitriding	1.10 (1.15)	1.3 (1.9)
Case hardening	1.1 (1.2)	1.2 (1.5)
Cold rolling	1.1 (1.2)	1.3 (1.5)
Shot peening	1.1 (1.1)	1.1 (1.4)
Inductive hardening, flame hardening	1.2 (1.3)	1.5 (1.6)

Fig. 3.11. Surface correction factors

lect for endurance limit value. The reasons for the conclusion are that the Shigley guideline is based on test data acquired in the 60s and are not updated periodically where FKM guideline is updated periodically since 1994. The temperature correction factor is very general for Shigley whereas it is very specifically provided in FKM to the requirement of this project. The size correction factor doesn't exist for dimensions beyond 10 inches which is a concern for developing the new tools of larger diameter. On the contrary, there is no maximum dimension limit for size factor provided by FKM. From the figure 3.11-3.13, we can observe the trend of correction factors amongst each other.

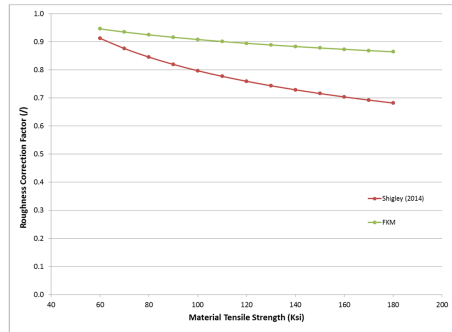


Fig. 3.12. Trend of roughness correction factor against Material tensile strength using Shigley 2014 and FKM guideline

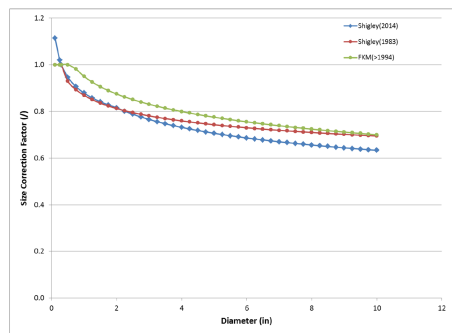


Fig. 3.13. Trend of size correction factor against diameter using Shigley 1983, Shigley 2014 and FKM guideline

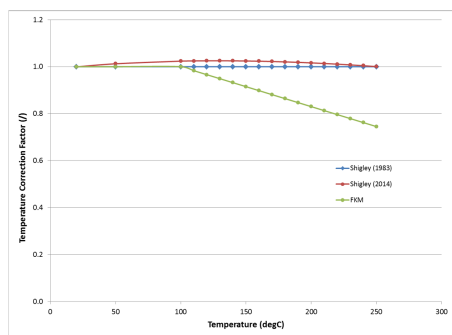


Fig. 3.14. Trend of temperature correction factor against temperature using Shigley 1983, Shigley 2014 and FKM guideline

3.5.3 Fatigue Failure Theories

Fatigue stress is defined as the weakening of any material caused due to cyclic loading. Fatigue causes localized structural damage. A proper design is thus nec-

essary to avoid failure due to fatigue. A generalized stress condition can be defined by combining purely reversing stress (a) with steady stress (m) [20]. If the stress is varying between σ_{max} σ_{min} , then:

$$\sigma_m = (\sigma_{max} + \sigma_{min})/2 \ \& \ \sigma_a = (\sigma_{max} - \sigma_{min})/2 \quad (3.15)$$

The diagram figure 3.14 for $\sigma_m \neq 0$, depicts an ideal case for stress representation of the LWD drill tool. On the x-axis, there is the number of life cycles and on the y-axis is the stress observed in the component. Here σ_m is mean stress acting due to torque and pressure and σ_a is stress amplitude for alternating stress acting due to bending moment.

- Ultimate Strength (S_{ut}): Stress level required to fail with one cycle
- Yield Strength (S_{yt}): Dividing line between elastic and plastic region
- Endurance Limit (S_e): If all cycles are below this stress level amplitude then no failures occur for infinite cycles

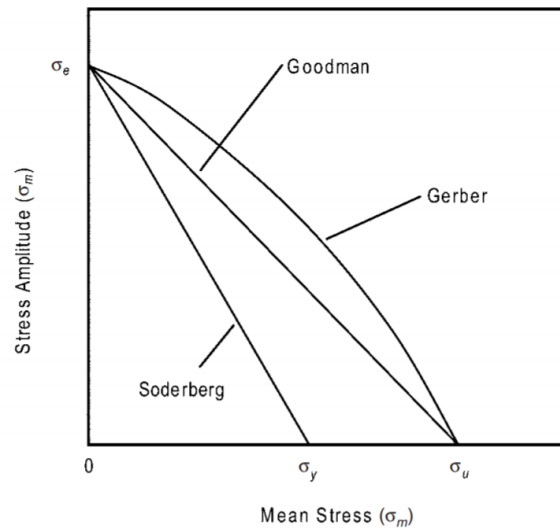


Fig. 3.15. Combined alternating and mean stress

As mentioned earlier there is no S-N data available for Inconel 718 and hence many stress theories can be considered to discover the danger zone that can lead to fatigue failure. To evaluate the design for alternating and mean stress, various stress theories are available. Depending upon the properties of the theories and its best fit to the situation for the given material and component, the following theories are discussed:

Where,

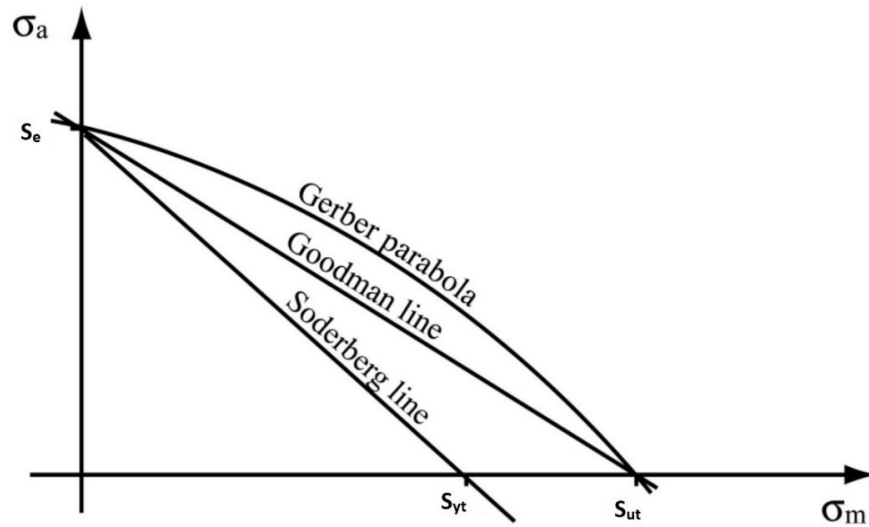


Fig. 3.16. Comparison of Soderberg, Goodman, and Gerber models

σ_m mean stress

σ_a - stress amplitude/alternating stress

S_{yt} tensile strength

S_{ut} ultimate tensile strength

S_e endurance limit

- Soderberg' s line:

When there is just reversing stress σ_a present, at that point for safe design Soderberg's line is used. Which means σ_a can go up to S_e when $\sigma_m = 0$. Soderberg Line is acquired by joining these two points. As shown in the figure, the Soderberg region is

contained between the combination of stresses and is defined by the Soderberg line, if the part lies in the contained region, it means it is unsafe [20]. The Soderberg's equation is given by:

$$\frac{\sigma_a}{S_e} + \frac{\sigma_m}{S_{yt}} \leq 1 \quad (3.16)$$

- Goodman's Line:

Goodman's relation is defined as the equation to quantify the way mean and alternating stress behave together where n is the fatigue life of a material. Goodman's line came into existence because of the brittle nature of the failure. As shown in the figure, Goodman suggested extending to S_{ut} instead of S_{yt} in Soderberg's equation. The resulting equation is:

$$\frac{\sigma_a}{S_e} + \frac{\sigma_m}{S_{ut}} \leq 1 \quad (3.17)$$

As can be seen from the equation, the Goodman Equation can be obtained easily from the Soderberg equation, by replacing S_{yt} with S_{ut} . Although Goodman's approach was valid when the magnitude of steady stress, m becomes more than S_{yt} , the part fails due to plastic deformation (the area is portrayed by the unsafe region). To eliminate this Modified Goodman's relation was introduced.

- Modified Goodman's Relation: A line is drawn at an angle of 45° angle from the S_{yt} point on the x-axis as shown in figure 3.12. A modified type of the Goodman relationship is suggested for general application under states of high-cycle fatigue. It is extremely conservative theory is advised to make the judgment of failed elements using more relaxed theory.

Mathematically, the Modified Goodmans equation should satisfy both the equations below:

$$\frac{\sigma_a}{S_e} + \frac{\sigma_m}{S_{ut}} = 1 \quad \& \quad \frac{\sigma_a}{S_e} + \frac{\sigma_m}{S_{yt}} = 1 \quad (3.18)$$

- Gerber Parabola:

Gerber came out with a parabolic approach to solve the S-N curves. The Gerber

parabola joins the X-axis, S_{ut} with the Y-axis, S_{yt} in a parabolic form as shown in the figure 3.16. The points show failure points which are test data points. Gerber equation is a parabolic equation given by:

$$\frac{\sigma_a}{S_e} + \frac{\sigma_m^2}{S_{ut}^2} \leq 1 \quad (3.19)$$

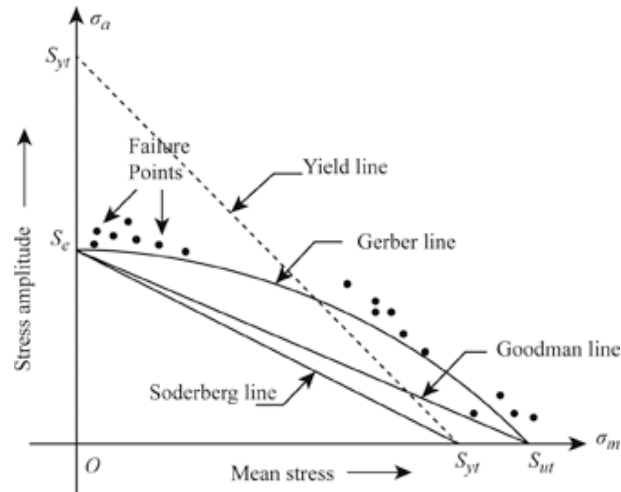


Fig. 3.17. Failure point depiction in the design of cyclic load

Observations:

Most real test data tend to fall between the Goodman and Gerber curves. For ductile material, the outcome of mean stress is improved from the Gerber line reflection. It is required to have a conservative approach for fatigue failure criteria along with the relaxed one. Thus, it is best suited to consider Goodman Line along with Gerber Line in order to make the decision for fatigue failure. Soderberg's equation Modified Goodman equation is seldom considered as it too conservative. If the coordinate obtained by the steady stress and the fluctuating stress falls under the arc given by the stress theory equations of Gerber and Goodman, then the part will survive.

4. FEA MODEL SETUP

4.1 FEA Model Set-up for Fatigue Analysis of the Drill Tool

The loading location and load magnitude details for the drill tool were provided by Halliburton. The loading provided is for static loading so static structural is selected for performing analysis.

4.2 Meshing of Elements

Meshing in a CAD system is the triangularization of a model to export it to other packages (render package, animation, etc.), discretization of a model into elements suitable for a FEM package and meshing of u- and v-parameter isocurves to let the user check the quality of a surface visually. The first step in meshing is an idealization of the CAD geometry. In most cases, this involves simplifying the model, removing details that are not relevant to the analysis, or that are likely to have a marginal impact on the results. It also involves cleaning-up or healing any defects in the CAD model.

Once the simulation model is ready, the next step is to use it to create the mesh. In the case of FEA, the mesh is embedded within and fitted to the body of the simulation model. There are different types of mesh elements, they can be 1D, 2D or 3D. The elements are mostly tetrahedral (3-sided pyramids), hexahedral (hexes or bricks), polyhedral (with any number of sides), prisms, or pyramids (with 5 sides).

In this paper, as the whole tool is symmetric, only one pocket is selected to fine mesh. There are two mesh sizing selected for the meshing. And since the critical area is relatively simpler a simple face mesh is applied for meshing the imaging pocket. The auto-generated mesh from Static structural with a face sizing mesh size of 0.1 in

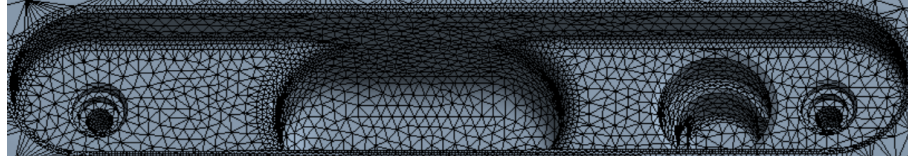
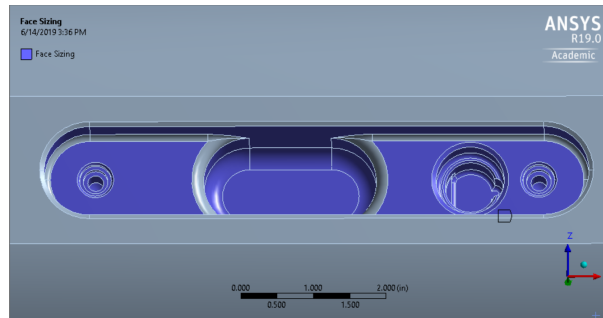


Fig. 4.1. Meshing of the LWD drill tool

and 0.05 in has been applied considering all the parameters like most accurate stress distribution, geometry dimensions, solver time and solver performance. The two sets of faces are as shown below:

Face sizing: The pocket is given finer mesh as compared to rest of the body as we need better results in that zone. Also, a finer mesh gives more symmetrical results after post-processing. There are 40 faces with the size of each element being 0.1 inches.



(a)

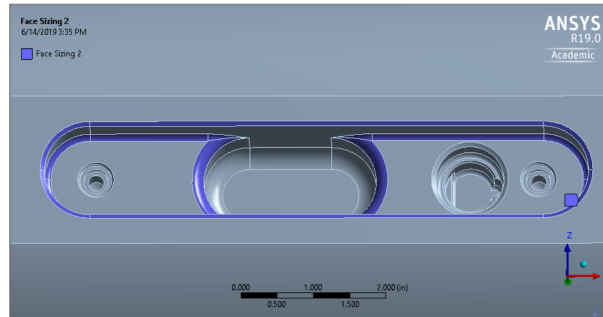
Scope	
Scoping Method	Geometry Selection
Geometry	48 Faces
Definition	
Suppressed	No
Type	Element Size
<input type="checkbox"/> Element Size	0.1 in
Advanced	
<input type="checkbox"/> Defeature Size	1.e-002 in
Behavior	Soft

(b)

Fig. 4.2. Face sizing of one imaging pocket in tension

Face sizing 2:

As can be seen from the figure 4.3, a finer mesh is created on the imaging pocket edges in comparison to the face sizing done. As known from the initial simulation that the selected face have critical stress accumulation. These faces require a higher level of mesh detail for generating proper results of stress. The number of faces which have such face sizing is 20 and the size of the elements is 0.05 inch.



(a)

Scope	
Scoping Method	Geometry Selection
Geometry	20 Faces
Definition	
Suppressed	No
Type	Element Size
<input type="checkbox"/> Element Size	5.e-002 in
Advanced	
<input type="checkbox"/> Defeature Size	Default
Behavior	Soft

(b)

Fig. 4.3. Face sizing 2 of one imaging pocket in tension

Named Selections:

This feature allows choosing any set of 3D entities. It helps to study the stress affected area of geometry more accurately. Taking advantage of symmetry, the result for various stresses and user-defined results are studied and scoped for only one named selection i.e. StressSurfaces for only one of the imaging pockets which is under tension. Following are the faces which are selected for studying fatigue failure and stress accumulation.

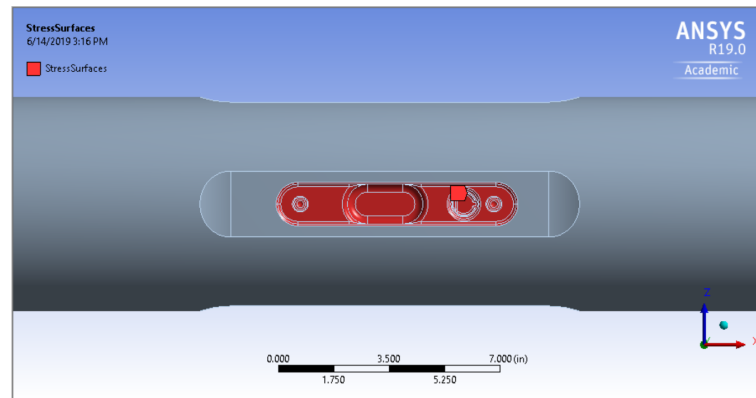
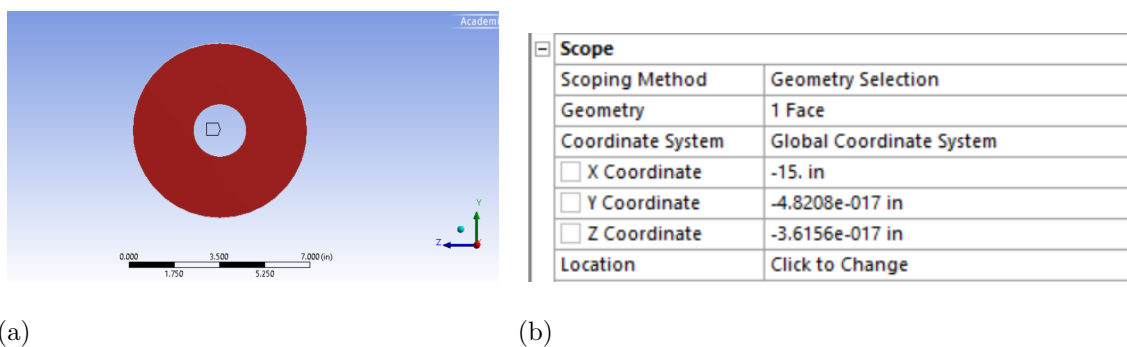


Fig. 4.4. Assignment of pocket through named selection

Remote point:

Remote points are a method of establishing a connection to the geometry, it can be in the form of a vertex, edge, face, body or a node, to a specific location in space. This association prevents an over-constraint situation that is likely to occur when multiple loads are applied to the same component or geometry. This greatly reduces the possibility of over-constraint. Here, one of the faces through which torque and bending moment are to be applied is selected for creating remote point as shown in figure 4.5.



(a)

(b)

Fig. 4.5. Assignment of remote point through face selection

Environment:

The figure 4.6 represents the environmental condition of the analysis.

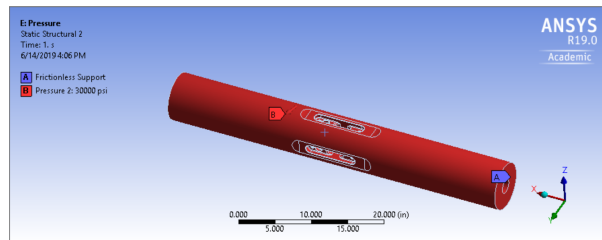
Definition	
Physics Type	Structural
Analysis Type	Static Structural
Solver Target	Mechanical APDL
Options	
<input type="checkbox"/> Environment Temperature	392. °F
<input type="checkbox"/> Generate Input Only	No

Fig. 4.6. Environmental Condition in Workbench Simulation

4.3 Boundary Conditions

- Pressure Only:

In this simulation, as shown in the figure, one end of the drill tool is applied for fixed support and a pressure load of 30,000 psi is applied throughout the tool as normal to the surface. The pressure here is steady stress and hence has a constant magnitude.



(a)

Scope	
Scoping Method	Geometry Selection
Geometry	288 Faces
Definition	
Type	Pressure
Define By	Normal To
Applied By	Surface Effect
<input type="checkbox"/> Magnitude	30000 psi (ramped)
Suppressed	No

(b)

Fig. 4.7. Boundary condition for pressure only simulation

- Bending Moment Only:

As shown in the figure 4.8, one end of the drill tool is applied as frictionless support. Frictionless support provides support such that the body is free to rotate and deform along tangential direction but not normal direction. A bending moment of $15^\circ/100ft$ is applied through tabular data 4.1 on the opposite face. The bending moment is the fluctuating stress here which acts only in Y-direction in the 1st time step, it acts in both Y and Z -direction at an angle of 45° to each of the axes [25]. For 2^{nd} time step and it acts only in the Z-direction for the 3rd time step 0.625 inches is the displacement of the face with respect to the central axis (x-axis) when a bending moment of $15^\circ/100ft$ is applied, with the property of symmetry only first quadrant of the Cartesian coordinates is studied whereas in 2^{nd} time step the magnitude is received by multiplying 0.625 with $\sin 45^\circ$ i.e. 0.4419.

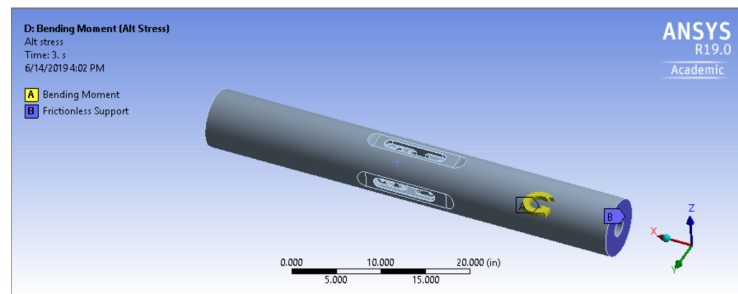


Fig. 4.8. Boundary condition for rotating bending simulation

Table 4.1.

Load steps for Alternating Stress applying through Bending Moment

Steps	Time[s]	RY[$^\circ$]	RZ[$^\circ$]
1	1	0.6250	0
2	2	0.4419	0.4419
3	3	0	0.6250

- Torque Only:

In this simulation, as shown in the figure, one end of the drill tool is selected for fixed support. And a torque of 35,000 lbf.ft is applied through a remote point on the opposite face. The torque is the steady stress here.

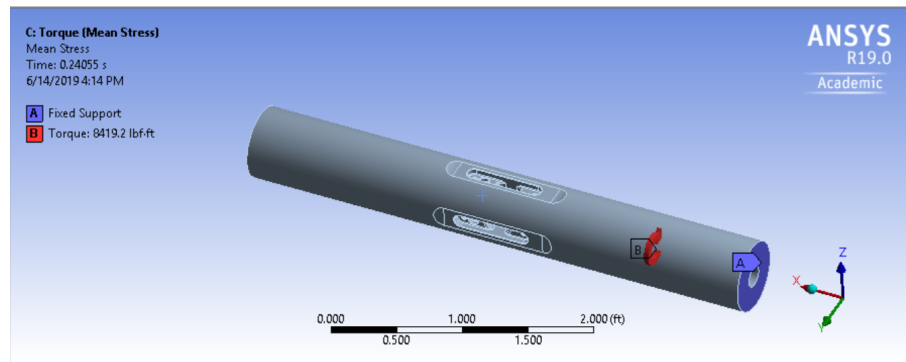
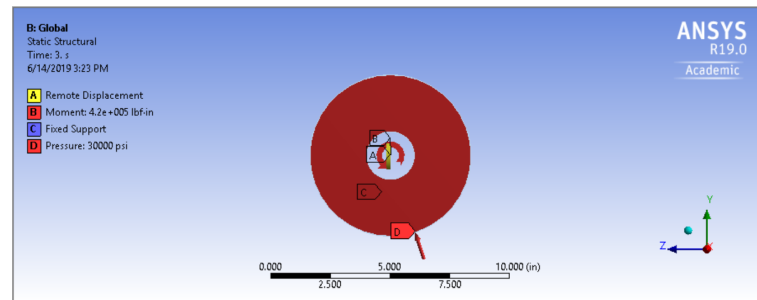


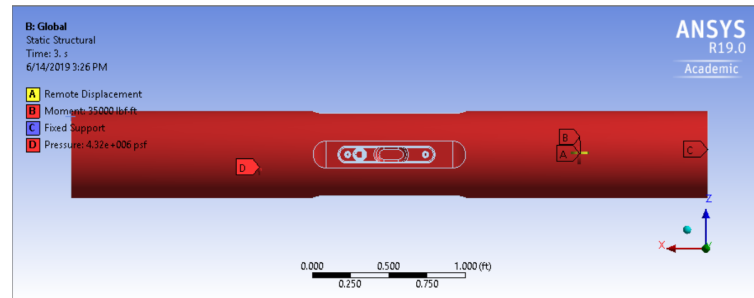
Fig. 4.9. Boundary condition for torque only simulation

- Global Model:

In the global model, all the three loads (pressure, bending moment and torque) are acting together. In the figure below it is seen in the side view that one end of the tool acts as fixed support and on the other end torque is applied via the remote point created earlier. Along with that pressure is applied to normal effect to surface (as shown in the figure 3.10) and bending moment is applied via a tabular data as a remote displacement to the face. The magnitude of forces acting is as follows 30,000 psi of pressure, 35,000 lbf.ft of torque and a bending moment of 15° degree/ 100ft.



(a)



(b)

Fig. 4.10. Images/Side view and Front view of boundary condition acting of the LWD tool for all three loads

4.4 Parameterization

The parameterization is done using ANSYS Workbench where various stress theories are calculated on the tool from the width ranging from 1.25 inch to a width of 2 inches (0.625 to 0.999 inches). Parameterization allows calculating the results for the manually entered design points without having to run a separate analysis for each design. The user-defined result like Gerber Theory, Goodman theory and factor of safety can be obtained for all 16 design points by the medium of parameterization. The values obtained are the maximum values for each design point and parameterization helps in finding all those values. Thus, the objective is achieved by performing the design of experiments (DOE). The above data in table 4.2 represents the result of fatigue stresses, stress theories, total deformation, and safety factor.

Table 4.2.
Data for different design point of the drill tool

Design Point	Fillet(in)	W	Alt. Stress	Gerber	Goodman	Def.Alt.(in)	Def.Mean(in)	Total Def. (in)	FS
DP 0	0.08	1.25	51979.05	1.045216	1.121961	0.00611	0.000597	0.112832	2.0920
DP 1	0.08	1.3	48234.68	0.969723	1.067174	0.005695	0.000603	0.112946	2.0397
DP 2	0.08	1.35	47861.7	0.962412	1.038673	0.005905	0.000609	0.113061	2.0478
DP 3	0.08	1.4	47293.73	0.951416	1.064817	0.005885	0.000614	0.113157	2.0299
DP 4	0.08	1.45	46862.36	0.942669	1.051465	0.008391	0.000621	0.113267	2.0524
DP 5	0.08	1.5	50143.73	1.007997	1.07985	0.006926	0.000628	0.113421	2.0382
DP 6	0.08	1.55	49389.32	0.994098	1.079842	0.005719	0.000635	0.113573	2.0147
DP 7	0.08	1.6	48651.41	0.979127	1.111313	0.005954	0.000643	0.113705	1.9937
DP 8	0.08	1.65	44675.34	0.901411	1.055296	0.007099	0.00065	0.11384	2.0016
DP 9	0.08	1.7	44841.12	0.904802	1.078749	0.005749	0.000658	0.113984	1.9769
DP 10	0.09	1.75	44591.99	0.899462	1.13132	0.010382	0.000666	0.114198	1.9952
DP 11	0.09	1.8	44353.33	0.894981	1.103757	0.005869	0.000676	0.11437	1.9843
DP 12	0.09	1.85	42800.59	0.864516	1.117636	0.006093	0.000685	0.114541	1.9608
DP 13	0.09	1.9	44525.66	0.89735	1.125231	0.006561	0.000694	0.114748	1.9457
DP 14	0.09	1.95	43644.98	0.879533	1.128824	0.007342	0.000705	0.114945	1.9343
DP 15	0.09	2.00	43250.34	0.934521	1.26847	0.005758	0.000716	0.115243	1.7801

1. The graph below shows the alternating stress characteristics of the imaging pocket with respect to the width of the imaging pocket. The endurance limit of the imaging pocket calculated from the FKM guidelines is found out to be 45595 psi, so any stress above the limit would result in fatigue of the pocket resulting in failure due to stress. In the graph, it is evident that the imaging pockets with width radius 0.625 in and 0.825 in will cause failure as their endurance limit is reached above 45595 psi.

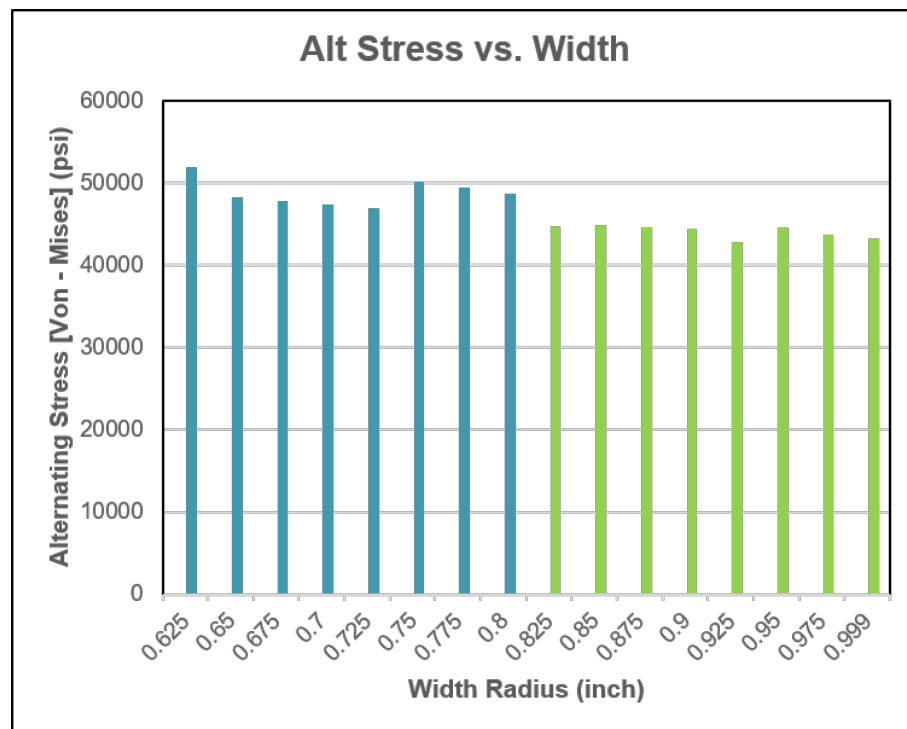


Fig. 4.11. Alternating stress vs Width of Imaging Pocket

2. The graph below shows the total deformation of the imaging pocket with respect to the width of the imaging pocket. The total deformation of the imaging pocket calculated from Ansys Workbench is found out to be more for alternating stress than mean stress. From the graph, it is evident that the total deformation is distinctively different for different design points.

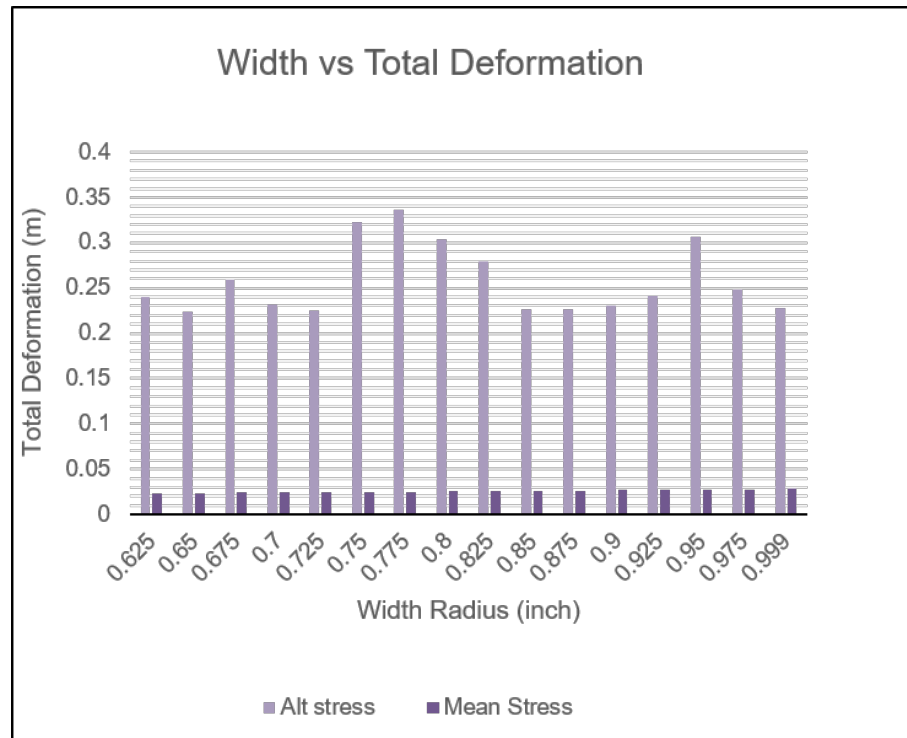


Fig. 4.12. Total Deformation vs Width of Imaging Pocket

3. The figure 4.13 below shows the Gerber and Goodman values in the Y-coordinate with respect to the width radius of the imaging pocket. As can be seen from the graph, all the values of Gerber and Goodman are above 0.8. The values are computed using Ansys Workbench and are complying to the respective relations of Gerber and Goodman criteria.
4. The figure 4.14 below shows the factor of safety with respect to the width radius of the imaging pocket. As can be seen from the graph, plastic failure occurs above a factor of safety of 1.5 and ultimate failure occurs at about a FOS of 2 for most of the radius. The factor of safety is a very important criterion in determining the fatigue of any component.

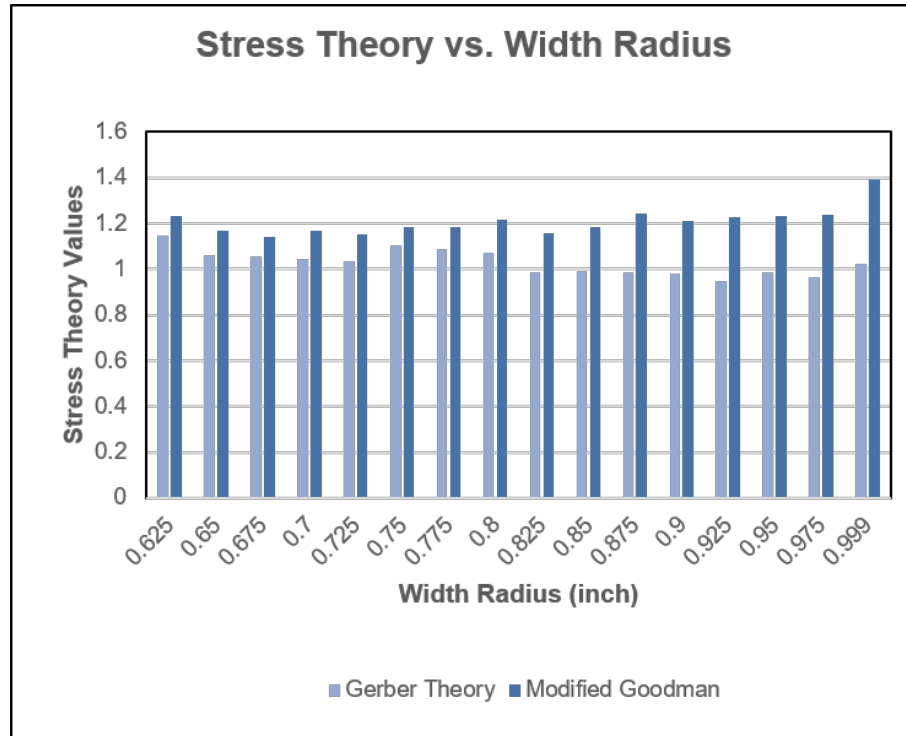


Fig. 4.13. Stress Life Theory vs Width of Imaging Pocket

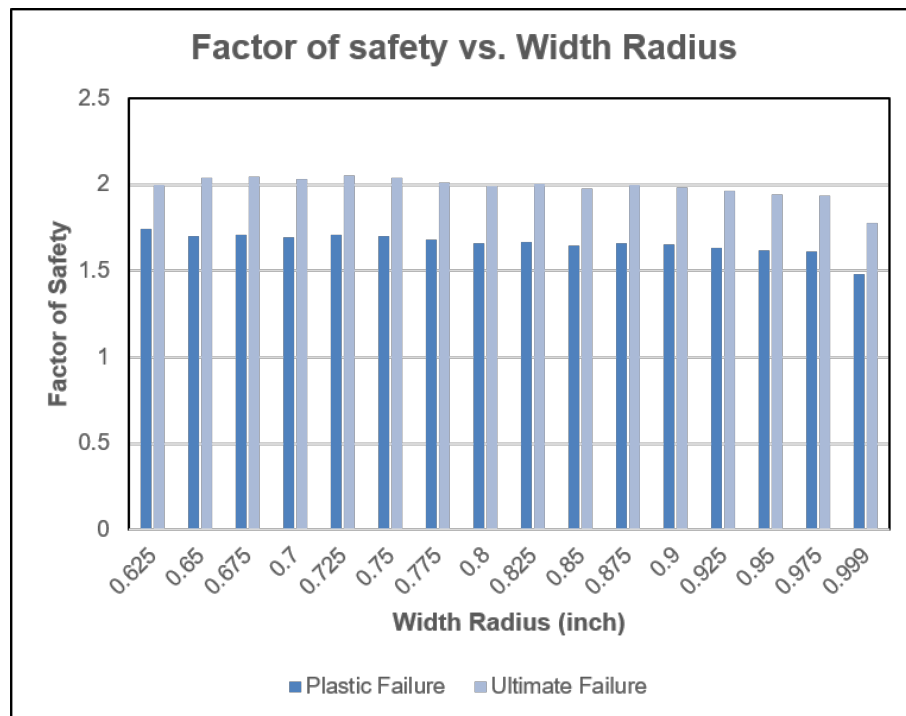


Fig. 4.14. Factor of Safety vs Width of Imaging Pocket

5. USER-DEFINED RESULTS AND CONCLUSION

The objective of this project of accommodating the largest possible transducer is achieved by varying the width of the imaging pocket. After analyzing the graphs of parameterization for width against alternating stress, stress theories, the factor of safety and total deformation, it can be concluded that the largest width possible without compromising its mechanical strength is 1.95 inches. To study the contour of stresses for the selected width, the 14th design point is set as current and the analysis is carried out using Workbench 19.0.

5.1 Global Model (Von – Mises Stress)

5.1.1 Equivalent Stress

As seen in the figure 5.1 the maximum stress observed in the imaging pocket is 93054 psi. As we know from the previous studies of 4.75 drill tool that stress concentration near the top surface chamfer of the imaging pocket should be avoided as it is a critical zone. It is evident in the figure below that the maximum stress no longer lies in the critical zone of the pocket. And, that the maximum stress is below the yield and ultimate strength of the material.

5.1.2 Total Deformation

As shown in the figure 5.2, due to the application of three types of loads which are pressure, bending moment and torque a deformation in the global loading condition takes place. The maximum deformation at the end opposite to the fixed support.

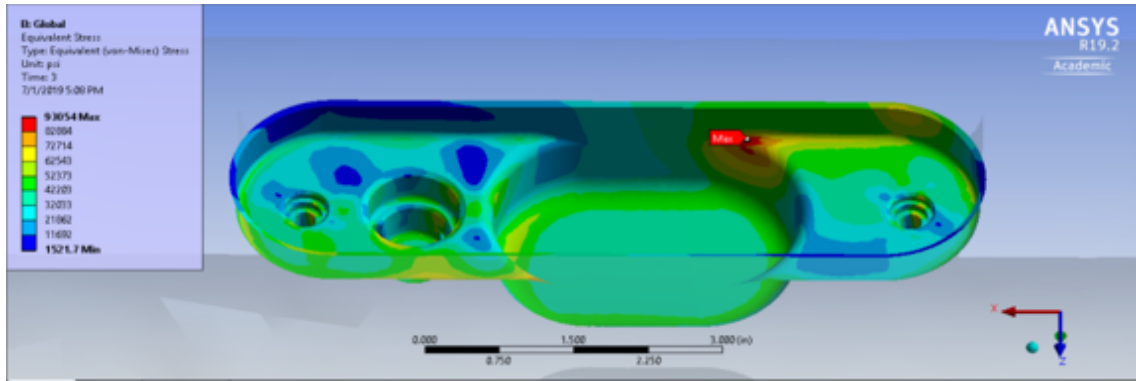


Fig. 5.1. Equivalent Stress due to Global loading condition

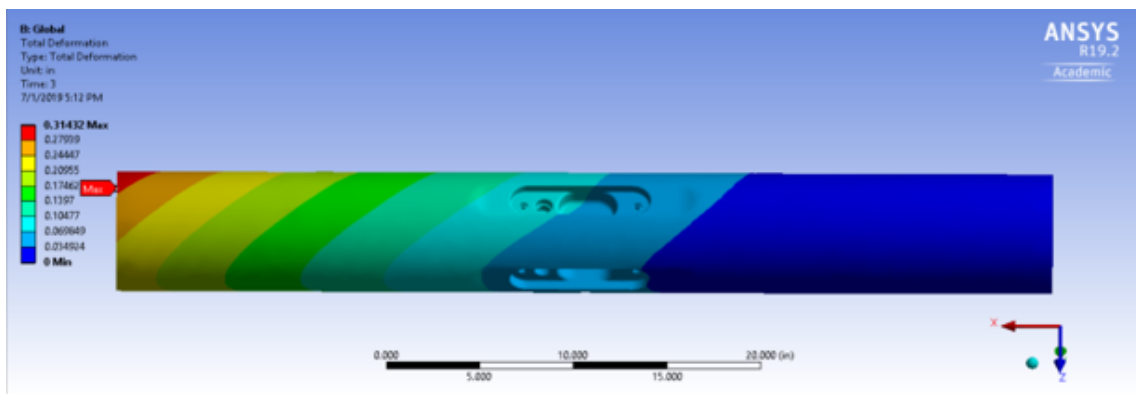


Fig. 5.2. Total deformation due to global loading

5.2 Torque Only Load

5.2.1 Equivalent Stress

The figure 5.3 below shows the equivalent stress due to torque on the imaging pocket. The torque is applied on the remote point of the free end and the maximum stress occurs on the threaded hole for the bolt as shown in the figure.

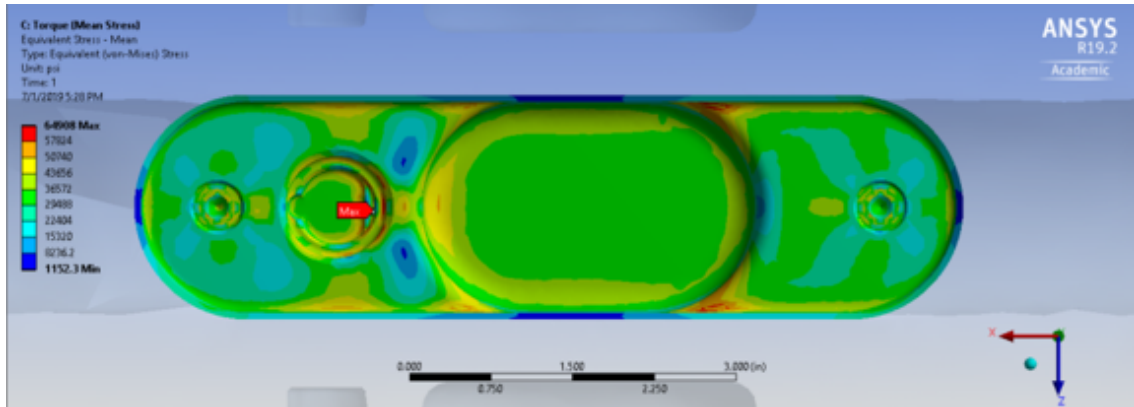


Fig. 5.3. Equivalent load due to torque only load (mean stress)

5.2.2 Total Deformation

Due to torque, there is a maximum total deformation occurring on the edge of the imaging pocket at the free end. The total deformation is inches in magnitude as shown in the figure below.

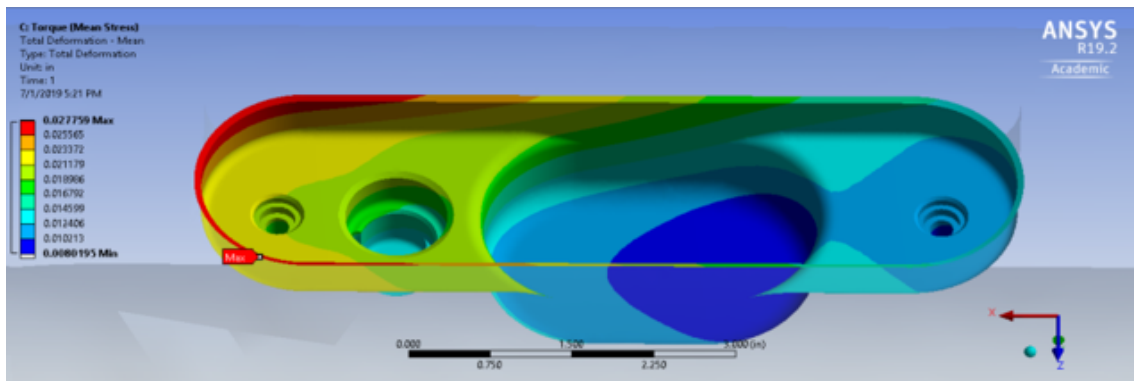


Fig. 5.4. Total deformation due to torque load

5.3 Bending Moment Only

5.3.1 Equivalent Stress

As shown in the figure below, the equivalent stress due to the bending moment, which is alternating stress, has a maximum value of 43654 psi on the threaded bolt region. This value is below 45595 psi which is the constraint of endurance limit. This means the product never fails as the value of equivalent stress is less than the endurance limit.

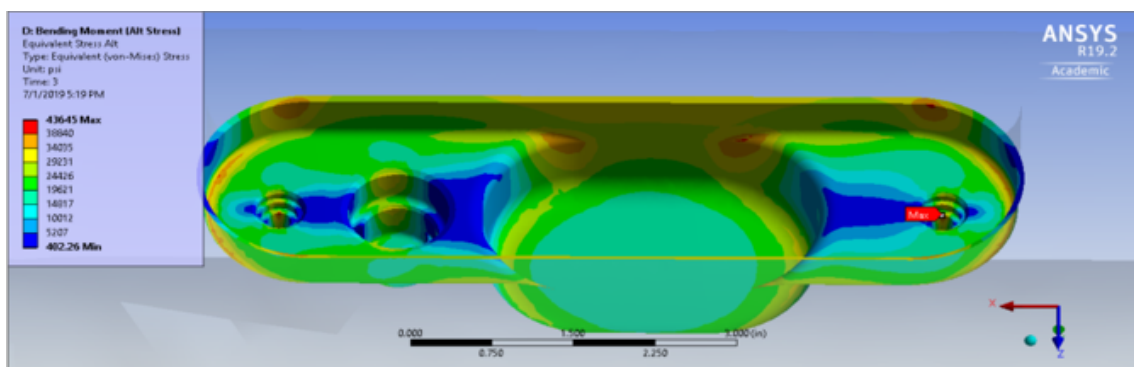


Fig. 5.5. Equivalent stress due to alternating load by bending moment

5.3.2 Total Deformation

The total deformation due to bending moment is maximum at one end and minimum at another end as shown in the figure. This change is for every time step as this is an alternating type of stress, so there will be a change in the total deformation as well. For $t=3s$, the maximum total deformation is 0.2481 inches.

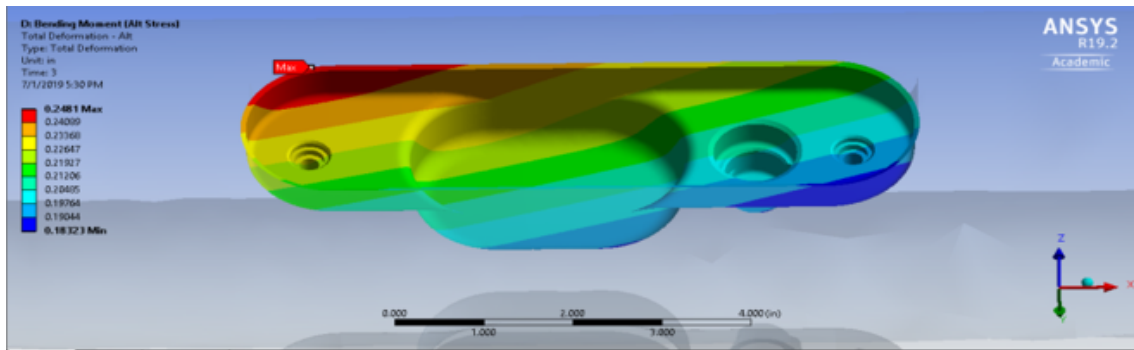


Fig. 5.6. Total deformation due to alternating load by bending moment

5.4 User Defined Results

5.4.1 Goodman Theory

If the coordinate given by the mean stress and the alternating stress lies under the curve given by the Goodman equation, then the part will survive. If the coordinate is above the curve, then the part will fail for the given stress parameters. Also from the equation, when rearranged in the form $\sigma_a / ((1 - (\sigma_m) / (S_{ut})) S_e) \leq 1$, should be less than or equal to 1 for a safe design.

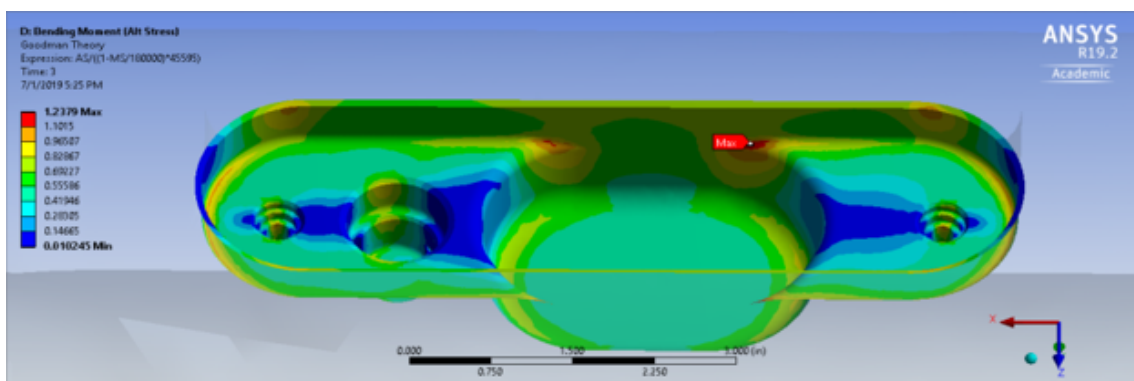


Fig. 5.7. Simulation result for the user-defined result of Goodman Theory

5.4.2 Gerber Theory

If the coordinate given by the mean stress and the alternating stress lies under the curve given by the Gerber equation, then the part will survive. If the coordinate is above the curve, then the part will fail for the given stress parameters. Also from the equation, when rearranged in the form $\sigma_a / ((1 - (\sigma_m) / (S_{ut})) S_e) \leq 1$, should be less than or equal to 1 for a safe design.

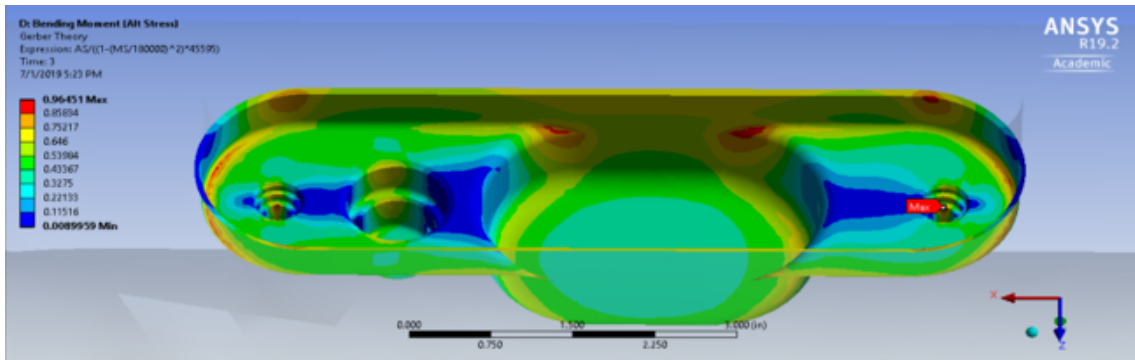


Fig. 5.8. Simulation result for the user-defined result of Goodman Theory

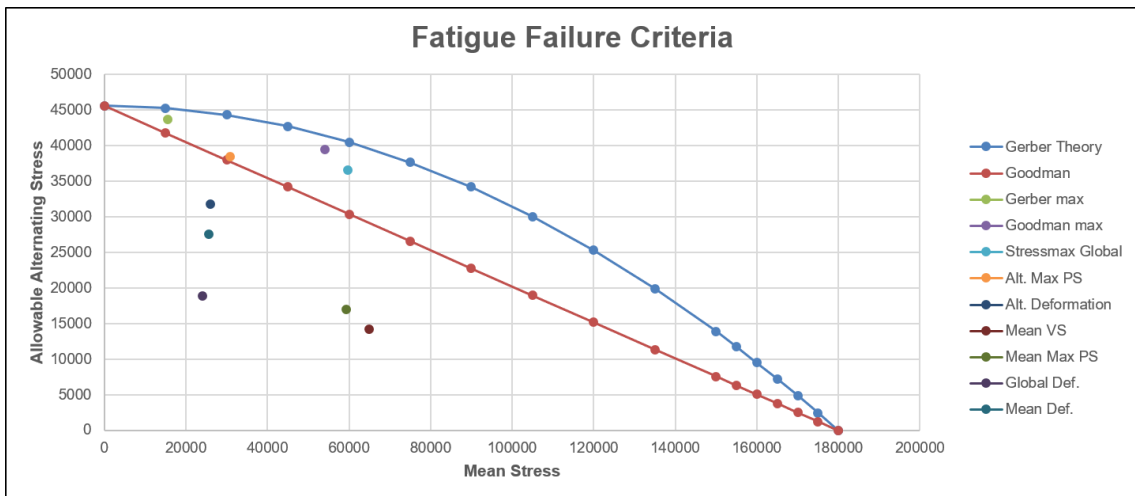


Fig. 5.9. Graphical Solution

5.5 Pressure Only

5.5.1 Equivalent Stress

As shown in the figure below, the minimum equivalent stress concentration due to pressure load is approximately 2.5×10^{-3} psi and the maximum equivalent stress concentration is 23.162 psi. However, the stress concentration is more inclined towards minimum stress in the imaging pocket which is a negligible quantity with respect to the steady stress generated by torque load. Hence the stress due to pressure is insignificant for the calculation of failure due to fatigue.

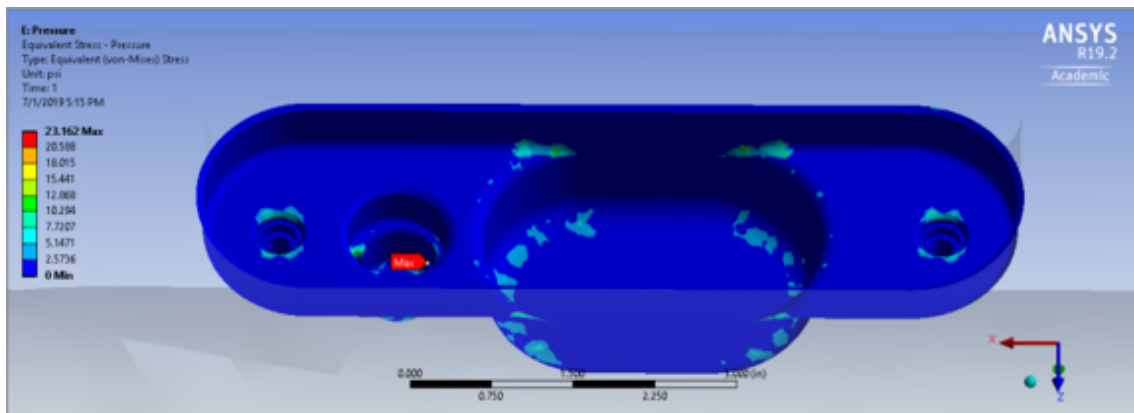


Fig. 5.10. Simulation result for the user-defined result of Goodman Theory

5.5.2 Total Deformation

The figure represents the total deformation occurring due to the pressure load. The end with the minimum deformation is fixed support and the opposite end is free, acting as a cantilever. Thus, the minimum deformation of 1.06×10^{-2} inches occurs near the fixed support and maximum deformation of 1.4×10^{-2} inches occurs at the free end.

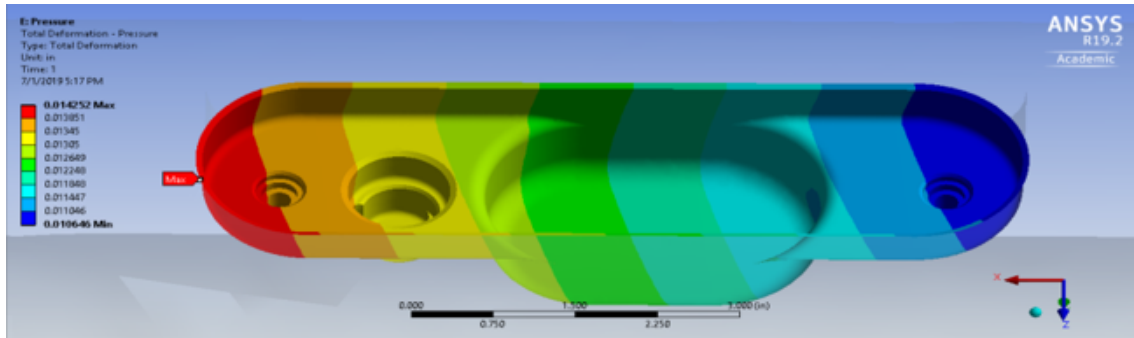


Fig. 5.11. Simulation result for the user-defined result of Goodman Theory

5.6 Limitations

There are few limitations to this fatigue analysis of the LWD drill tool. The Limitations are discussed below:

1. Vibration Analysis: Vibration fatigue is not considered in this analysis. Only Static Fatigue is analysed in this situation as vibration is a dynamic load and requires static dynamic loading for the solving the setup. PSD, dynamic power spectral density is used for analysing fatigue caused due to vibration.
2. Validation: Validating the process through experimental comparison requires data from industry and research institutes which are of proprietary values. Building a physical prototype can included as future work with support of lab resources.
3. Prototype: This project is limited in terms of building large scale prototype of the drill tool.
4. Loading: Non-Proportional loading is beyond the scope of this project as FKM guideline does not support the particular type of loading.

REFERENCES

REFERENCES

- [1] K. Mozie, "Characterization of ultrasonic waves in various drilling fluids," University College of Southeast Norway, Tech. Rep., 2017.
- [2] Schlumberger, "Logging-while-drilling (lwd)," accessed on July 23, 2019. [Online]. Available: https://en.wikipedia.org/wiki/Logging_while_drilling
- [3] M. Morys, R. Chemali, G. Goodman, G. Smollinger, B. Schaecher, and V. Maki, "Field testing of an advanced lwd imager for oil-based mud applications," *SPWLA 51st Annual Logging Symposium*, 2010.
- [4] I. Dowell, M. Andrew, and L. Matt, "Measurement-while-drilling (mwd)," accessed on July 23, 2019. [Online]. Available: https://en.wikipedia.org/wiki/Measurement_while_drilling
- [5] Halliburton, "Logging-while-drilling (lwd)," accessed on July 23, 2019. [Online]. Available: <https://www.halliburton.com/en-US/ps/sperry/drilling/lwd.html>
- [6] M. Prammer, M. Morys, S. Knizhnik, C. Conrad, W. Hendricks, M. Bittar, G. Hu, F. Hveding, K. Kenny, R. Shokeir, D. Seifert, S. Al-Dossari, and P. Neumann, "A high-resolution lwd resistivity imaging tool field testing in vertical and highly deviated boreholes," *OnePetro*, vol. 50, pp. 49–66, 2009.
- [7] G. Kirby, "The effect of transducer size, shape and orientation on the resolution of boundary layer pressure fluctuations at a rigid wall," *The journal of sound and vibration*, vol. 10, 1969.
- [8] V. Maki, S. Gianzero, R. Strickland, N. Kepple, and G. Mark, "Dynamically focused transducer applied to the cast imaging tool," *SPWLA 32nd Annual Logging Symposium*, 1991.
- [9] S. Gupta, *Constant Amplitude Stress-Life Analysis*, accessed on July 23, 2019. [Online]. Available: <https://www.efatigue.com/constantamplitude/stresslife/#a>
- [10] H. Tengyue, Z. Zhaoyang, S. Sheng, Y. Yang, and Z. Chenhui, "The fatigue life analysis of turbine blades in the air cycle machine," 2017.
- [11] S. Zamani, S. Hassanzadeh-Tabrizi, and H. Sharifi, "Failure analysis of drillpipe a review," *Science Direct*, 2015.
- [12] B. Lui, Z. Zhu, J. Zhang, W. Lei, and B. Wu, "Fatigue failure analysis of drilling tools for ultra-deep wells in shunbei block," *Materials Science and Engineering*, 2018.
- [13] K. Anandavel, R. Prakash, and A. Davis, "Effect of preloading on the contact stress distribution of a dovetail interface," *International Journal of Mechanical, Aerospace, Industrial, Mechatronic and Manufacturing Engineering*, 2010.

- [14] S. Pandey, “Fea analysis and optimization of differential housing for fatigue stresses and fatigue test design to study skin effect in ductile iron,” Michigan Technological University, Tech. Rep., 2015.
- [15] high temperature metals, “Inconel 718 technical data,” accessed on July 23, 2019. [Online]. Available: <https://www.hightempmetals.com/techdata/hitempInconel718data.php>
- [16] probabilistic engineering design, “Introduction to design optimization,” accessed on July 23, 2019. [Online]. Available: <http://web.mst.edu/~dux/repository/me360/ch10.pdf>
- [17] E. Osakue, L. Anetor, and C. Odetunde, “Fatigue shaft design verification for bending and torsion,” *International Journal of Engineering Innovation Research*, vol. 4, 2015.
- [18] Y. L. Lee and D. Taylor, “Stress-based fatigue analysis and design. in fatigue testing and analysis,” SAE Technical Papers, Tech. Rep., 2005.
- [19] S. Gupta, *Design for Cyclic Loading*, accessed July 20, 2019. [Online]. Available: https://web.njit.edu/~sengupta/met%20301/cyclic_loading%20indefinite.pdf
- [20] R. Budynas and J. K. Nisbett, “Shigley’s mechanical engineering design,” pp. 265–344, 2015.
- [21] C. R. Mischke, “Prediction of stochastic endurance strength. trans. of asme,” *Journal of Vibration, Acoustics, Stress, and Reliability in Design*, pp. 113–122, 1987.
- [22] J. Shigley and L. Mitchell, “Mechanical engineering design,” pp. 400–450, 1983.
- [23] S. McKelvey, Y.-L. Lee, and M. Barkey, “Stress-based uniaxial fatigue analysis using methods described in fkm-guideline,” pp. 445–484, 2012.
- [24] D. C. Defense, “Mcdonnell,” accessed on July 23, 2019. [Online]. Available: <https://apps.dtic.mil/dtic/tr/fulltext/u2/431618.pdf>
- [25] R. Hammer, H. Suryadi, Y. Tao, W. Qian, and R. Mokhti, “Managing bha integrity with bha design based on bending moment and stress analysis,” vol. 2, pp. 951–961, 2016.